

Analysis of Intensity of Singular Stress Field for Bonded Cylinder and Bonded Pipe in Comparison with Bonded Plate

Tatsujiro Miyazaki ^{a*}, Nao-Aki Noda ^{b*}, Fei, Ren ^b, Zefeng Wang ^b, Yoshikazu Sano ^b, Kazuki Iida ^b

^a Department of Mechanical Systems Engineering, University of the Ryukyus, 1 Senbaru, Nishihara-cho, Nakagami-gun, Okinawa 903-0213, Japan

^b Department of Mechanical Engineering, Kyushu Institute of Technology, 1-1 Sensui-cho, Tobata-ku, Kitakyushu-shi, Fukuoka 804-8550, Japan

*Corresponding author:

Tatsujiro Miyazaki, Department of Mechanical Systems Engineering, University of the Ryukyus, 1 Senbaru, Nishihara-cho, Nakagami-gun, Okinawa 903-0213, Japan, Tel: +81-98-895-8609, E-mail: t-miya@tec.u-ryukyu.ac.jp

Nao-Aki Noda, Department of Mechanical Engineering, Kyushu Institute of Technology, 1-1 Sensui-cho, Tobata-ku, Kitakyushu-shi, Fukuoka 804-8550, Japan, Tel: +81-93-884-3124, E-mail: noda@mech.kyutech.ac.jp

Abstract

In this paper, the intensity of the singular stress field (ISSF) for a bonded cylinder and bonded pipe is compared with the ISSF for the bonded plate. The analysis method focuses on the FEM stress at the interface end by applying the same mesh pattern to the unknown and reference problems. It is found that the mesh-independent technique useful for the bonded plate cannot be directly applied to the bonded axisymmetric structures because the circumferential strain causes non-singular stress disturbs singular stress evaluation. In order to eliminate this disturbance, explicit non-singular expressions are derived from the boundary conditions and subtracted from the FEM results. Then, the ISSFs for the bonded cylinder and the bonded pipe are calculated by changing the material combinations systematically. Since Dundurs' parameters cannot totally control the axisymmetric bonded structures, the maximum and minimum values of ISSF are shown in tables and charts under arbitrary material combination. It is found that the ISSFs of bonded cylinder and bonded pipe are at most 1.5 times larger than that of the bonded plate.

Keyword

Interfaces, Finite element stress analysis, Joint design, Fracture mechanics, Intensity of singular stress field

Nomenclature

a	radius of bonded cylinder	α, β	Dundurs' parameters
d	radius of bonded cylinder	$\varepsilon_{\theta\theta}^{CYL}$	real circumferential strain of bonded cylinder
E	Young's modulus		
e_{\min}	minimum element size	$\varepsilon_{j0,FEM}^{CYL}, \gamma_{r z0,FEM}^{CYL}$	FEM strain of bonded cylinder at interface end

$F_{\sigma_z}^{CBJ}$	Normalized ISSF for cylindrical butt joint	$\varepsilon_{i0,FEM}^{PLT}, \gamma_{xy0,FEM}^{PLT}$	FEM strain of bonded plate at interface end
$F_{\sigma_j}^{CYL}, F_{\tau_{rz}}^{CYL}$	Normalized ISSF for bonded cylinder	λ	singular index
$F_{\sigma_j}^{PIP}, F_{\tau_{rz}}^{PIP}$	Normalized ISSF for bonded pipe	ν	Poisson's ratio
$F_{\sigma_i}^{PLT}, F_{\tau_{xy}}^{PLT}$	Normalized ISSF for bonded plate	$\sigma_i^{BJ}, \tau_{xy}^{BJ}$	real stress of butt joint
G	shear modulus	$\sigma_j^{CYL}, \tau_{rz}^{CYL}$	real stress of bonded cylinder
$K_{\sigma_i}^{BJ}, K_{\tau_{xy}}^{BJ}$	ISSF for butt joint	$\sigma_i^{PLT}, \tau_{xy}^{PLT}$	real stress of bonded plate
$K_{\sigma_z}^{CBJ}$	ISSF for cylindrical butt joint	$\sigma_{i0,FEM}^{BJ}, \tau_{xy0,FEM}^{BJ}$	FEM stress of butt joint at interface end
$K_{\sigma_c}^{CBJ}$	Critical ISSF for cylindrical butt joint at debonding fracture	$\sigma_{j0,FEM}^{CYL}, \tau_{rz0,FEM}^{CYL}$	FEM stress of bonded cylinder at interface end
$K_{\sigma_j}^{CYL}, K_{\tau_{rz}}^{CYL}$	ISSF for bonded cylinder	$\sigma_{j0,FEM}^{PIP}, \tau_{rz0,FEM}^{PIP}$	FEM stress of bonded pipe at interface end
$K_{\sigma_j}^{PIP}, K_{\tau_{rz}}^{PIP}$	ISSF for bonded pipe	$\sigma_{\sigma_i}^{PLT}, K_{\tau_{xy}}^{PLT}$	ISSF for bonded plate
$K_{\sigma_i}^{PLT}, K_{\tau_{xy}}^{PLT}$	ISSF for bonded plate	$\sigma_{i0,FEM}^{PLT}, \tau_{xy0,FEM}^{PLT}$	FEM stress of bonded plate at interface end
L, l	plate length and cylinder length	$\tilde{\sigma}_{j0,FEM}^{CYL}, \tilde{\tau}_{rz0,FEM}^{CYL}$	non-singular FEM stress of bonded cylinder at interface end
R	distance from the end on the interface	$\tilde{\sigma}_{j0,FEM}^{PIP}, \tilde{\tau}_{rz0,FEM}^{PIP}$	non-singular FEM stress of bonded pipe at interface end
t	adhesive layer thickness of butt joint	$\sigma_y^{\infty}, \sigma_z^{\infty}$	uniform applied stress
u_{r0}^{CYL}	real radial displacement of bonded cylinder	ρ	inner radius of the bonded pipe
$u_{r0,FEM}^{CYL}$	FEM radial displacement of bonded cylinder		
W	plate width		

1. Introduction

Adhesive bonding is used in various industries such as automobiles, marines and airplanes on account of developments of high performance adhesives [1 - 3]. The structural adhesives have several advantages such as high fatigue strength, weight reduction, high sealability and high productivity compared to welding, bolts and screws [1]. In general, the structural adhesive is developed so that the adhesive strength becomes higher than the static strength of the structural materials such as steels and aluminum alloys. However, when the debonding fracture occurs at the interface between the adhesive and the adherend, the adhesive strength decreases remarkably. It is therefore important to grasp the debonding strength. Although the experimental evaluation methods have been standardized by ASTM, ISO and JIS, the debonding strength cannot be estimated conveniently. This is because the adhesive strength is prescribed by the fracture load regardless of the fracture modes in those standards. Therefore, a convenient method for evaluating the debonding strength is strongly required.

In the previous studies [4 - 11], the debonding strength of the adhesively bonded joints was expressed by the intensity of the singular stress field (ISSF). The ISSF K_{σ} for the butt joint as shown in Fig. 1 is defined by the following equation.

$$K_{\sigma} = \sigma_y^{\infty} F_{\sigma} W^{1-\lambda} = \lim_{R \rightarrow 0} R^{1-\lambda} \sigma_y \quad (1)$$

Here, σ_y^{∞} is the remote stress, F_{σ} is the normalized ISSF, λ is the singular index, W is the plate width, R is the local distance from the interface edge and σ_y is the stress in the y direction. To calculate the ISSF, a mesh-independent technique was proposed by the authors [7, 8]. Then, the debonding strength of the adhesive joint was expressed as $K_{\sigma} = K_{\sigma_c}$ [9 - 11] for the butt joints in Fig. 1 [7, 8] and the single lap joints [9]. Here, K_{σ} denotes the ISSF and K_{σ_c} denotes the critical value of ISSF. As can be seen in those studies [4 - 11], the debonding strength can be predicted from the two dimensional modeling although actual specimens have three dimensional geometries. However, since actual specimens are always three dimensional, 3D effect on the ISSF should be studied.

In this study, therefore, the bonded cylinder (Fig. 3(a)) and the bonded pipe (Fig. 3(b)) will be considered as the most fundamental 3D bonded structures, which should be compared with the bonded plate in the first place. Under the same material combination, the ISSF can be compared among those three problems since the same singular index and the similar singular stress field appears [12]. In this study, the same FE mesh pattern will be applied for the bonded plate in Fig. 2 and the bonded cylinder in Fig. 3 as well as the bonded pipe. Then, the analytical differences will be discussed by comparing with those FE results. Since it is known that the non-singular stress occurs at the interface end for the axisymmetric bonded structures [13 - 15], the applicability of the mesh-independent technique has to be considered to analyze the bonded cylinder and the bonded pipe accurately. Then, the analysis method will be newly proposed for the bonded axisymmetric bodied. Finally, the ISSFs for the bonded cylinder and the bonded pipe will be calculated by varying the material combinations. Quite generally, the bonded pipe has been regarded as the bonded plate when the inner radius of the bonded pipe ρ approaches ∞ . Therefore, the singular stress fields between the bonded pipe and the bonded plate will be discussed as the most fundamental 3D and 2D problems.

2. A mesh-independent technique useful for evaluating the ISSF for bonded cylinder and bonded pipe

2.1 Stress/strain continuity or discontinuity across the interface

The method of analysis will be explained for bonded cylinder. The bonded pipe can be analyzed in a similar way. Fig. 2 shows the schematic illustration of the bonded plate and Fig. 3 shows the one of bonded cylinder. The dimensions are set as $L=W=2a$ in those models. Table 1 shows an example of a bad pair satisfying $\alpha(\alpha-2\beta)>0$ to explain the analysis method. Note that Table 1 is just an example to analyze all material combinations whose results are indicated in Figs. 7, 12 and Tables 6, 7, 10, 11. Table 1 includes Young's modulus E_1, E_2 , Poisson's ratio ν_1, ν_2 , Dundurs' [16] parameters (α, β) and singular index λ . Here, the subscript m differentiates the material 1 and material 2. The parameters (α, β) are defined by Eq. (2). For the bad pair $\alpha(\alpha-2\beta)>0$, it is known that the singular stress field $\lambda < 1$ appears at the interface end.

By using the material combination shown in Table 1, the analysis method will be examined for Fig. 2 and Fig. 3 in this Sect. 2. After the validity is confirmed, the method will be applied to all material combinations for bonded cylinder as shown in Sect. 3 and bonded pipe as shown in Sect. 4.

$$\alpha = \frac{G_1(\kappa_2 + 1) - G_2(\kappa_1 + 1)}{G_1(\kappa_2 + 1) + G_2(\kappa_1 + 1)} \quad (2a)$$

$$\beta = \frac{G_1(\kappa_2 - 1) - G_2(\kappa_1 - 1)}{G_1(\kappa_2 + 1) + G_2(\kappa_1 + 1)} \quad (2b)$$

Here, $\kappa_m = 3 - 4\nu_m$. Then, λ value is obtained by solving the following eigenequation [12, 17, 18].

$$\left[\sin^2\left(\frac{\pi}{2}\lambda\right) - \lambda^2 \right]^2 \beta^2 + 2\lambda^2 \left[\sin^2\left(\frac{\pi}{2}\lambda\right) - \lambda^2 \right] \alpha\beta + \lambda^2(\lambda^2 - 1)\alpha^2 + \frac{\sin^2(\pi\lambda)}{4} = 0 \quad (3)$$

Figure 8 shows (α, β) for several engineering material combinations [19]. Since in most cases (α, β) is in the range of $0 \leq \beta \leq 0.3$ included in the bad pair region $\alpha(\alpha - 2\beta) > 0$, the parameters in Table 1 were chosen from the bad pair region as typical example. The parameters are not real material parameters.

In this analysis, the commercial FEM code MSC Marc 2008 R1 is used. The linear elastic analyses are performed on the bonded plate as shown in Fig. 2 and the bonded cylinder as shown in Fig. 3. The multifrontal method is used in the solution of simultaneous equations. In the case of the bonded plate, the plane strain condition is assumed. Figure 4 shows the schematic illustration of the FE mesh pattern. The same FE mesh patterns are used in all analyses. The standard four-node quadrilateral plane strain and axisymmetric ring elements are used for the bonded plate and the bonded cylinder, respectively. In order to confirm the usefulness of the mesh independent technique, the FE analyses are performed by using the coarse mesh and the fine mesh. The minimum element sizes are $e_{\min}/(W/2) = e_{\min}/a = 3^{-9}$ for the coarse mesh and 3^{-12} for the fine mesh.

Table 2 shows the stress/strain components of the bonded cylinder under the remote stress $\sigma_z^\infty = 1$, $(\sigma_{j0,FEM}^{CYL}, \tau_{rz0,FEM}^{CYL}, \varepsilon_{j0,FEM}^{CYL}, \gamma_{rz0,FEM}^{CYL})$, and the stress/strain components of the bonded plate under the remote stress $\sigma_y^\infty = 1$, $(\sigma_{i0,FEM}^{PLT}, \tau_{xy0,FEM}^{PLT}, \varepsilon_{i0,FEM}^{PLT}, \gamma_{xy0,FEM}^{PLT})$, where $j = r, z, \theta$ and $i = x, y, z$. The stress/strain values are the nodal solutions obtained by FE analyses and they are referred to as ‘‘FEM stress/strain’’. In Table 2, the values in the parentheses are the singular components and the non-singular components that will be explained in Sect. 2.3. The real stress/strain components $(\sigma_r^{CYL}, \sigma_\theta^{CYL}, \varepsilon_z^{CYL}, \gamma_{rz}^{CYL})$, $(\sigma_x^{PLT}, \sigma_z^{PLT}, \varepsilon_y^{PLT}, \gamma_{xy}^{PLT})$ are discontinuous across the interface, but the components $(\sigma_z^{CYL}, \tau_{rz}^{CYL}, \varepsilon_r^{CYL}, \varepsilon_\theta^{CYL})$, $(\sigma_y^{PLT}, \tau_{xy}^{PLT}, \varepsilon_x^{PLT}, \varepsilon_z^{PLT})$ must be continuous across the interface. However, in the FEM analysis even the continuous-should-be stress/strain components $(\sigma_{z0,FEM}^{CYL}, \tau_{rz0,FEM}^{CYL}, \varepsilon_{r0,FEM}^{CYL}, \varepsilon_{\theta0,FEM}^{CYL})$, $(\sigma_{y0,FEM}^{PLT}, \tau_{xy0,FEM}^{PLT}, \varepsilon_{x0,FEM}^{PLT}, \varepsilon_{z0,FEM}^{PLT})$ of the materials 1 and 2 do not always coincide with each other because of the FEM error. In this case, average values for the materials 1 and 2 are used and indicated in Table 2.

In Table 2, most of the stress/strain components are mesh-dependent except for ε_θ . This can be explained in the following way. In axisymmetric bodies, the circumferential strain ε_θ is given as [20]:

$$\varepsilon_\theta = \frac{u_r}{r}, \quad (4)$$

where r is the radial distance from the z axis, u_r is the displacement in the r direction. The circumferential strain at the interface end $\varepsilon_{\theta0}^{CYL}$ is given by Eq. (5) from the cylinder radius a and the displacement at the interface end u_{r0}^{CYL} .

$$\varepsilon_{\theta0}^{CYL} = \frac{u_{r0}^{CYL}}{a} \quad (5)$$

Table 3 shows the $\varepsilon_{\theta 0, FEM}^{CYL}$ values calculated by substituting the FEM radial displacement $u_{r0, FEM}^{CYL}$ into Eq. (5). The $\varepsilon_{\theta 0, FEM}^{CYL}$ value obtained from $u_{r0, FEM}^{CYL}$ is -0.5137 independent of the element size e_{min} , and coincides with the FEM stress in Table 2. Usually, the stress and strain at the singular point cannot be calculated by FEM accurately. However, the only $\varepsilon_{\theta 0, FEM}^{CYL}$ is not influenced by the stress singularity and can be calculated accurately by FE analysis.

As shown in Table 2 and Table 3, $\varepsilon_{\theta 0}^{CYL}$ for the bonded cylinder has a non-zero value and quite different from ε_{z0}^{PLT} for the bonded plate. This is the reason why the non-singular stress/strain components are caused by $\varepsilon_{\theta 0}^{CYL}$. Therefore, the FEM stress at the interface end consists of the singular stress and the non-singular stress. Since $\varepsilon_{\theta 0}^{CYL}$ is not affected by the stress singularity and it can be calculated easily and accurately.

2.2 Mesh-independent technique useful for analyzing bonded plate

In the earlier studies [7, 8, 11], the ISSFs for the butt joints in Fig. 1 and the bonded plate in Fig. 2 were calculated accurately. In this section, first, the same analysis method is applied to the bonded cylinder as shown in Fig. 3 by FEM, then the analytical difficulty for bonded cylinder and pipe will be clarified. For Fig. 1 and Fig. 2, the singular stress at the end of interface is expressed as shown in the following equations.

$$\sigma_i^{PLT} = \frac{K_{\sigma_i}^{PLT}}{R^{1-\lambda}}, \quad \tau_{xy}^{PLT} = \frac{K_{\tau_{xy}}^{PLT}}{R^{1-\lambda}} \quad (6)$$

$$\sigma_i^{BJ} = \frac{K_{\sigma_i}^{BJ}}{R^{1-\lambda}}, \quad \tau_{xy}^{BJ} = \frac{K_{\tau_{xy}}^{BJ}}{R^{1-\lambda}} \quad (7)$$

Here, the index i can be x , y or z , R is the distance from the end on the interface. Since those singular stress fields are similar as shown in Eqs (6) and (7), the ISSF ratio is equal to the stress ratio obtained by FEM as shown in Eq. (8) [7, 8, 11].

$$\frac{K_{\sigma_y}^{BJ}}{K_{\sigma_y}^{PLT}} = \frac{\lim_{R \rightarrow 0} R^{1-\lambda} \sigma_y^{BJ}}{\lim_{R \rightarrow 0} R^{1-\lambda} \sigma_y^{PLT}} = \lim_{R \rightarrow 0} \frac{\sigma_y^{BJ}}{\sigma_y^{PLT}} = \frac{\sigma_{y0, FEM}^{BJ}}{\sigma_{y0, FEM}^{PLT}} \quad (8)$$

In other words, the error of FEM stress $\sigma_{y0, FEM}^{PLT}$ and $\sigma_{y0, FEM}^{BJ}$ can be cancelled out by taking the ratio. It was shown that Eq. (8) is valid to the other stress components, and therefore all stress ratios have the same value independent of the stress components. The method does not require the special singular element such as Akin singular element and the mesh refinement procedure for the convergence of the solution. Since the reference solution $K_{\sigma_y}^{PLT}$ was obtained by the body force method (BFM) [21] and the FEM error can be eliminated in Eq. (8), the present method has the same accuracy as the BFM.

Table 4 shows the FEM results of the bonded cylinder and butt joint. Here, $l = L$, $l/W = 1.0$ and $t/l = 0.1$ are set in the butt joint model (Fig. 1). The butt joint and the bonded plate are subdivided by the same mesh pattern and analyzed under the same conditions and the same material combinations by FEM. The stress ratios of the butt joint and the bonded cylinder are also shown in Table 4. Although the non-singular stress components will be derived in the following Sect. 2.3 explicitly, the singular and non-singular components are shown in Table 4 beforehand so that the existence of the non-singular components can be confirmed at a glance. All ratios of the butt joint correspond to 0.6674 and are independent of the mesh pattern. From this result, it is confirmed that the

influence of the stress singularity is cancelled completely by taking a ratio and the mesh refinement procedure for the convergence of the solution is not required. In the case of the bonded cylinder, the $\sigma_{r0,FEM}^{CYL} / \sigma_{x0,FEM}^{PLT}$ and $\tau_{rz0,FEM}^{CYL} / \tau_{xy0,FEM}^{PLT}$ correspond to 0.9948. However, the other ratios $\sigma_{\theta0,FEM}^{CYL} / \sigma_{z0,FEM}^{PLT}$ and $\sigma_{z0,FEM}^{CYL} / \sigma_{y0,FEM}^{PLT}$ do not correspond to 0.9948. That is because the non-singular stresses as mentioned in Sect. 2.1 are included in the FEM stresses $\sigma_{z0,FEM}^{CYL}$ and $\sigma_{\theta0,FEM}^{CYL}$ cannot be ignored.

2.3 Derivation of the non-singular stresses

In this section, the asymptotic solution of the stress distribution in the vicinity of the interface end of the bonded cylinder is discussed based on theory of elasticity. In order to distinguish from FE analysis, the notation's subscript excludes "FEM". The non-singular stresses explained in Sect. 2.1 are denoted by $\tilde{\sigma}_j^{CYL}$ and $\tilde{\tau}_{rz}^{CYL}$, where $j = r, z, \theta$. The interface stresses σ_j^{CYL} and τ_{rz}^{CYL} can be expressed as shown in Eq. (9) at the vicinity of the interface end of the bonded cylinder. Note that the bonded plate and the bonded cylinder have the same singular index λ .

$$\sigma_j^{CYL} = \frac{K_{\sigma_j}^{CYL}}{R^{1-\lambda}} + \tilde{\sigma}_j^{CYL}, \quad \tau_{rz}^{CYL} = \frac{K_{\tau_{rz}}^{CYL}}{R^{1-\lambda}} + \tilde{\tau}_{rz}^{CYL} \quad (9)$$

From the interfacial continuity conditions for the stress and the displacement, Eq. (9) has to be satisfied with the following conditions at the interface between the materials 1 and 2.

$$\left(\sigma_z^{CYL}\right)^1 = \left(\sigma_z^{CYL}\right)^2, \quad \left(\tau_{rz}^{CYL}\right)^1 = \left(\tau_{rz}^{CYL}\right)^2 \quad (10)$$

$$\left(u_r^{CYL}\right)^1 = \left(u_r^{CYL}\right)^2, \quad \left(u_\theta^{CYL}\right)^1 = \left(u_\theta^{CYL}\right)^2 \quad (11)$$

Here, the subscripts 1 and 2 refer to the materials 1 and 2, respectively. From the stress-free boundary conditions at $r = a$, Eq. (9) also has to be satisfied with the following conditions at the interface end on both materials.

$$\left(\sigma_r^{CYL}\right)^1 = \left(\tau_{rz}^{CYL}\right)^1 = 0 \dots (z \geq 0) \quad (12)$$

$$\left(\sigma_r^{CYL}\right)^2 = \left(\tau_{rz}^{CYL}\right)^2 = 0 \dots (z \leq 0) \quad (13)$$

Two right-hand side terms of Eq. (9) have to be satisfied with the conditions (10), (11), (12) and (13) independently. The non-singular stresses were solved analytically by Li et al. [15]. In this paper, such non-singular stresses as meet the conditions and cause the strain $\varepsilon_{\theta\theta}^{CYL} = u_{r0}^{CYL} / a$ are derived.

From the stress-free conditions (12) and (13), the non-singular stresses at the interface end, $\tilde{\sigma}_{r0}^{CYL}$ and $\tilde{\tau}_{rz0}^{CYL}$, are equal to 0 on both materials.

$$\left(\tilde{\sigma}_{r0}^{CYL}\right)^1 = \left(\tilde{\tau}_{rz0}^{CYL}\right)^1 = 0 \quad (14)$$

$$\left(\tilde{\sigma}_{r0}^{CYL}\right)^2 = \left(\tilde{\tau}_{rz0}^{CYL}\right)^2 = 0 \quad (15)$$

Letting $\left(\tilde{\sigma}_{z0}^{CYL}\right)^1 = \left(\tilde{\sigma}_{z0}^{CYL}\right)^2 = \tilde{\sigma}_{z0}^{CYL}$ from the condition (10) leads the following relation from $\left(\varepsilon_{r0}^{CYL}\right)^1 = \left(\varepsilon_{r0}^{CYL}\right)^2$

which is effected by Eq. (11).

$$\left(\frac{\nu_1}{E_1} - \frac{\nu_2}{E_2}\right) \tilde{\sigma}_{z^0}^{CYL} = -\frac{(\tilde{\sigma}_{\theta 0}^{CYL})^{\dagger}}{E_1} + \frac{(\tilde{\sigma}_{\theta 0}^{CYL})^2}{E_2} \quad (16)$$

Similarly, the following relation can be obtained from $(\varepsilon_{\theta 0}^{CYL})^{\dagger} = (\varepsilon_{\theta 0}^{CYL})^2$ which is effected by Eq. (11).

$$\left(\frac{\nu_1}{E_1} - \frac{\nu_2}{E_2}\right) \tilde{\sigma}_{z^0}^{CYL} = \frac{\nu_1}{E_1} (\tilde{\sigma}_{\theta 0}^{CYL})^{\dagger} - \frac{\nu_2}{E_2} (\tilde{\sigma}_{\theta 0}^{CYL})^2 \quad (17)$$

Solving Eqs. (5), (16) and (17), the $(\tilde{\sigma}_{\theta 0}^{CYL})^{\dagger}$ and $(\tilde{\sigma}_{\theta 0}^{CYL})^2$ are obtained as:

$$(\tilde{\sigma}_{\theta 0}^{CYL})^{\dagger} = \frac{(1+\nu_2)(\nu_2 E_1 - \nu_1 E_2) E_1}{(1+\nu_1)\nu_1 E_2 - (1+\nu_2)\nu_2 E_1} \cdot \frac{u_{r0}^{CYL}}{a}, \quad (18)$$

$$(\tilde{\sigma}_{\theta 0}^{CYL})^2 = \frac{(1+\nu_1)(\nu_2 E_1 - \nu_1 E_2) E_2}{(1+\nu_1)\nu_1 E_2 - (1+\nu_2)\nu_2 E_1} \cdot \frac{u_{r0}^{CYL}}{a}. \quad (19)$$

Then, the $(\tilde{\sigma}_{z^0}^{CYL})^{\dagger}$ and $(\tilde{\sigma}_{z^0}^{CYL})^2$ are obtained as:

$$(\tilde{\sigma}_{z^0}^{CYL})^{\dagger} = (\tilde{\sigma}_{z^0}^{CYL})^2 = -\frac{(\nu_1 - \nu_2) E_1 E_2}{(1+\nu_1)\nu_1 E_2 - (1+\nu_2)\nu_2 E_1} \cdot \frac{u_{r0}^{CYL}}{a}. \quad (20)$$

The equivalent expressions were obtained by Lie et al [15]. The non-singular stresses are uniquely determined from the displacement u_{r0}^{CYL} in the radial direction. The non-singular stresses can be calculated by Eqs. (14), (15), (18), (19) and (20). The mesh-independent technique [7, 8] is applicable to the bonded cylinder by subtracting the non-singular stress from the FEM stress. However, when $\alpha = 2\beta$, the denominators of the equations become 0 and the non-singular stresses diverge to ∞ . The full attention is required when $\alpha = 2\beta$, which will be discussed in Section 3.

2.4 Mesh-independent technique useful for analyzing bonded cylinder and bonded pipe

The non-singular stress components were derived explicitly in Sect. 2.3. In this section the usefulness and the validity will be discussed by taking an example of the results of Tables 1 - 4. Table 5(a) shows the non-singular stresses obtained from $u_{r0,FEM}^{CYL}$ by using explicit Eqs. (14), (15), (18), (19), (20) in Sect.2.3. Here, the radial displacement $u_{r0,FEM}^{CYL}$ and the non-singular FEM stresses are independent of the minimum element size e_{\min} as shown in Table 5(a). Table 5(b) shows the singular stresses by subtracting the non-singular stresses in Table 5(a) from the stresses at the interface end in Table 2. The singular FEM stress components in Table 5 (b) are depending on the mesh size. Table 5(c) shows the ratios of the bonded cylinder over the bonded plate by excluding the non-singular stress in Table 5(a). In Table 5(c), all components have the same ratio 0.9948 independent of the element size e_{\min} quite differently from Table 4(a). Because the $\sigma_{r0,FEM}^{CYL}$ and $\tau_{rz0,FEM}^{CYL}$ do not include the non-singular stresses as $\tilde{\sigma}_{r0,FEM}^{CYL} = \tilde{\tau}_{rz0,FEM}^{CYL} = 0$, the subtraction process is not necessary. Therefore, by using $\sigma_{r0,FEM}^{CYL}$ and $\tau_{rz0,FEM}^{CYL}$, the ratio of the ISSF for the bonded cylinder to the bonded plate can be calculated easily.

The ISSF for the bonded plate with $L/W = 1$ as shown in Fig. 2, $K_{\sigma_v}^{PLT}$, has been solved by Noda et al. [21]. Then, the non-dimensional function of θ has been already clarified by Carpenter and Byers [22]. Therefore, the

ISSFs for the bonded cylinder, $K_{\sigma_j}^{CYL}$ and $K_{\tau_{rz}}^{CYL}$ can be calculated from $K_{\sigma_r}^{CYL}/K_{\sigma_x}^{PLT} = K_{\sigma_z}^{CYL}/K_{\sigma_y}^{PLT} = K_{\sigma_\theta}^{CYL}/K_{\sigma_z}^{PLT} = K_{\tau_{rz}}^{CYL}/K_{\tau_{xy}}^{PLT} = 0.9948$. Table 5(d) shows the dimensionless ISSFs for the bonded plate and the bonded cylinder, where the $F_{\sigma_i}^{PLT}$ and $F_{\tau_{xy}}^{PLT}$, $F_{\sigma_j}^{CYL}$ and $F_{\tau_{rz}}^{CYL}$ are defined by Eqs. (21) and (22). The $F_{\sigma_j}^{CYL}$ and $F_{\tau_{rz}}^{CYL}$ have three significant digits as well as the $F_{\sigma_i}^{PLT}$ and $F_{\tau_{xy}}^{PLT}$.

$$F_{\sigma_i}^{PLT} = \frac{K_{\sigma_i}^{PLT}}{\sigma_y^\infty W^{1-\lambda}}, \quad F_{\tau_{xy}}^{PLT} = \frac{K_{\tau_{xy}}^{PLT}}{\sigma_y^\infty W^{1-\lambda}}, \quad (21)$$

$$F_{\sigma_j}^{CYL} = \frac{K_{\sigma_j}^{CYL}}{\sigma_z^\infty (2a)^{1-\lambda}}, \quad F_{\tau_{rz}}^{CYL} = \frac{K_{\tau_{rz}}^{CYL}}{\sigma_z^\infty (2a)^{1-\lambda}}. \quad (22)$$

As for the bonded cylinder, the stresses on the interface in the vicinity of the interface end can be described as follows.

$$\sigma_j^{CYL} = \frac{K_{\sigma_j}^{CYL}}{R^{1-\lambda}} + \tilde{\sigma}_{j0}^{CYL}, \quad \tau_{rz}^{CYL} = \frac{K_{\tau_{rz}}^{CYL}}{R^{1-\lambda}} + \tilde{\tau}_{rz0}^{CYL} \quad (23)$$

Table 5(e) shows the $\sigma_{z,FEM}^{CYL}$ along the R coordinate in Fig. 3 in comparison with the $\sigma_{y,FEM}^{PLT}$ in Fig. 2. Also the ratio of the $(\sigma_{z,FEM}^{CYL} - \tilde{\sigma}_{z0,FEM}^{CYL})$ to the $\sigma_{y,FEM}^{PLT}$ along the R coordinate, $(\sigma_{z,FEM}^{CYL} - \tilde{\sigma}_{z0,FEM}^{CYL})/\sigma_{y,FEM}^{PLT}$, is shown in Table 5(e). By subtracting the non-singular term, the ratio is constant at 0.9948 along the R coordinate and has four significant digits as shown in Table 5(e). The ISSF is calculated accurately by Eq. (24). Only the FEM stresses at the interface end are enough to obtain the ratio.

$$\frac{K_{\sigma_z}^{CYL}}{K_{\sigma_y}^{PLT}} = \frac{\sigma_{z0,FEM}^{CYL} - \tilde{\sigma}_{z0,FEM}^{CYL}}{\sigma_{y0,FEM}^{PLT}} \quad (24)$$

Equation (24) can be used to obtain other stress components. Since the derivation of the non-singular stresses is quite general, the present method can be applied to analyzing other axisymmetric bodies such as bonded pipes and cylindrical butt joints. As an example of adhesive joint specimens, the cylindrical butt joint is analyzed accurately in Appendix A. The present method is useful for the engineers and the researchers to evaluate the debonding strength easily and conveniently.

3. Intensity of singular stress field for bonded cylinder in comparison with bonded plate

In our earlier studies [8, 9], the ISSFs for the bonded plate and the butt joint have been clarified under arbitrary material combinations. In this paper, the ISSFs for the bonded cylinder and the bonded pipe will be discussed in a similar way. The singular stress field of two dimensional problems in Figs. 1 and 2 is totally controlled by Dundurs' parameters (α, β) regardless of the plane stress condition or the plane strain condition. However, the singular stress field of axisymmetric problems such as the bonded cylinder in Fig. 3 is a 3D problem and cannot be controlled by (α, β) . Since the axisymmetric bonded problems have some similarities to 2D bonded problems, the usefulness of (α, β) to the axisymmetric bonded problems will be examined.

Figure 5 shows E_2/E_1 and ν_2 by varying ν_1 from 0 to 0.5 when $(\alpha, \beta) = (0.8, 0.3)$. As shown in Figs. 5 (a) and 5(b), under fixed $(\alpha, \beta) = (0.8, 0.3)$ E_2/E_1 can be changed from 0.1074 to 0.1389 and ν_2 can be changed from 0.1818 to 0.2500. Then, $\sigma_{z0,FEM}^{CYL}/\sigma_{y0,FEM}^{PLT}$ and $K_{\sigma_z}^{CYL}/K_{\sigma_y}^{PLT}$ are calculated as shown in Fig. 5 (c) by using the fine mesh pattern of the standard four-node quadrilateral element with $e_{\min}/a = 3^{-12}$. Since mesh-independent technique [7, 8] is used, singular elements such as Akin singular element are not necessary. Here,

$K_{\sigma_z}^{CYL}/K_{\sigma_y}^{PLT}$ is obtained by using Eq. (24) for the bad pair. For the good and equal pairs, however, since the singular stress does not appear, $\sigma_{z0,FEM}^{CYL}/\sigma_{y0,FEM}^{PLT}$ will be focused in order to compare the bonded cylinder and the bonded plate. It is found that $\sigma_{z0,FEM}^{CYL}/\sigma_{y0,FEM}^{PLT}$ changes from 0.962 to 1.066 and $K_{\sigma_z}^{CYL}/K_{\sigma_y}^{PLT}$ changes from 0.957 to 1.087. For axisymmetric bonded structures, although (α, β) cannot totally control the results, it is found that the variation is not very large as shown in Fig. 5(c). In this paper, therefore, the maximum and minimum values will be focused under fixed (α, β) . To evaluate the bonded structures under arbitrary material combination, the maximum value is important since this is the most severe case under the same (α, β) .

Figure 6 shows the maximum values of $K_{\sigma_z}^{CYL}/K_{\sigma_y}^{PLT}$ and $\sigma_{z0,FEM}^{CYL}/\sigma_{y0,FEM}^{PLT}$ by varying α from 0.2 to 1.0 for fixed $\beta = 0.3$. For the bad pair $\alpha(\alpha - 2\beta) > 0$, the solid line indicates the ISSF ratio $(K_{\sigma_z}^{CYL})_{\max}/K_{\sigma_y}^{PLT}$ and the broken line indicates the stress ratio $(\sigma_{z0,FEM}^{CYL}/\sigma_{y0,FEM}^{PLT})_{\max}$. For the good pair $\alpha(\alpha - 2\beta) < 0$, the solid line indicates $(\sigma_{z0,FEM}^{CYL}/\sigma_{y0,FEM}^{PLT})_{\max}$ and for the equal pair $\alpha(\alpha - 2\beta) = 0$, the open circle mark indicates the $(\sigma_{z0,FEM}^{CYL}/\sigma_{y0,FEM}^{PLT})_{\max}$. When $\alpha > 2\beta$, the stress singularity occurs at the interface end, and therefore, $K_{\sigma_z}^{CYL}/K_{\sigma_y}^{PLT}$ may be useful for predicting the debonding strength. On the other hand, when $\alpha \leq 2\beta$, the stress singularity does not occur at the interface end. Then, it is found that $(K_{\sigma_z}^{CYL})_{\max}/K_{\sigma_y}^{PLT} \rightarrow \infty$ as $\alpha \rightarrow 2\beta$. However, as shown in Fig. 6(b), the singular stress field disappears since the index $\lambda \rightarrow 1$ as $\alpha \rightarrow 2\beta$. Therefore, the stress ratio $(\sigma_{z0,FEM}^{CYL}/\sigma_{y0,FEM}^{PLT})_{\max}$ may be more useful than the ISSF ratio $K_{\sigma_z}^{CYL}/K_{\sigma_y}^{PLT}$ around $\alpha = 2\beta$. In Fig. 6(c), the dimensionless ISSF $F_{\sigma_y}^{PLT}$ defined in Eq. (21) is also indicated.

Figure 7 and Tables 6, 7 show the maximum and minimum values of $K_{\sigma_z}^{CYL}/K_{\sigma_y}^{PLT}$ and $\sigma_{z0,FEM}^{CYL}/\sigma_{y0,FEM}^{PLT}$ by varying (α, β) . As above mentioned, $K_{\sigma_z}^{CYL}/K_{\sigma_y}^{PLT}$ may be useful for predicting the debonding strength when $\alpha(\alpha - 2\beta) > 0$ since the singular stress appears at the interface end. On the other hand, when $\alpha(\alpha - 2\beta) \leq 0$, $\sigma_{z0,FEM}^{CYL}/\sigma_{y0,FEM}^{PLT}$ is very important for predicting the debonding strength. However, when $\alpha \cong 2\beta$, it is unknown whether $K_{\sigma_z}^{CYL}/K_{\sigma_y}^{PLT}$ or $\sigma_{z0,FEM}^{CYL}/\sigma_{y0,FEM}^{PLT}$ is suitable for predicting the strength because $(K_{\sigma_z}^{CYL})_{\max}/K_{\sigma_y}^{PLT}$ goes to ∞ as $\alpha \rightarrow 2\beta$.

Although $(K_{\sigma_z}^{CYL})_{\max}/K_{\sigma_y}^{PLT}$ goes to infinity around the equal pair condition, $(K_{\sigma_z}^{CYL})_{\max}/K_{\sigma_y}^{PLT}$ is less than 1.5 in the region $\alpha(\alpha - 2k\beta) \geq 0$, $k = 1.35 - 0.7|\beta|$ indicated in Fig. 8.

$$\frac{(K_{\sigma_z}^{CYL})_{\max}}{K_{\sigma_y}^{PLT}} \leq 1.5 \quad \text{for most of the bad pair } \alpha(\alpha - 2k\beta) \geq 0, \quad k = 1.35 - 0.7|\beta| \quad \text{in Fig. 8} \quad (25)$$

As shown in Fig. 8, since almost all (α, β) of engineering materials [19] are distributed in $0 \leq |\beta| \leq 0.3$, the stress ratio $\sigma_{z0,FEM}^{CYL}/\sigma_{y0,FEM}^{PLT}$ can be discussed in this range. Note that the stress ratio $(\sigma_{z0,FEM}^{CYL}/\sigma_{y0,FEM}^{PLT})_{\max}$ is always finite. Comparing Fig. 7(a) with Fig. 7(b), it is found that the value of $\sigma_{z0,FEM}^{CYL}/\sigma_{y0,FEM}^{PLT}$ varies depending on (α, β) but the value range of $(\sigma_{z0,FEM}^{CYL}/\sigma_{y0,FEM}^{PLT})_{\max}$ is not very wide in the region $\alpha(\alpha - 2\beta) \leq 0$ and $0 \leq |\beta| \leq 0.3$. Also, the difference between $(\sigma_{z0,FEM}^{CYL}/\sigma_{y0,FEM}^{PLT})_{\max}$ and $(\sigma_{z0,FEM}^{CYL}/\sigma_{y0,FEM}^{PLT})_{\min}$ is not very large in this region. Therefore, the value range and the maximum and minimum value difference can be expressed in Eq. (26).

$$1.0 \leq \left(\frac{\sigma_{z0,FEM}^{CYL}}{\sigma_{y0,FEM}^{PLT}} \right)_{\max} \leq 1.5, \quad \frac{\left(\frac{\sigma_{z0,FEM}^{CYL}}{\sigma_{y0,FEM}^{PLT}} \right)_{\max} - \left(\frac{\sigma_{z0,FEM}^{CYL}}{\sigma_{y0,FEM}^{PLT}} \right)_{\min}}{\left(\frac{\sigma_{z0,FEM}^{CYL}}{\sigma_{y0,FEM}^{PLT}} \right)_{\max} + \left(\frac{\sigma_{z0,FEM}^{CYL}}{\sigma_{y0,FEM}^{PLT}} \right)_{\min}} \leq 0.1 \quad (26)$$

for most of the good pair $0 \leq |\beta| \leq 0.3$ and $\alpha(\alpha - 2\beta) < 0$

If the differences between $\left(\sigma_{z0,FEM}^{CYL} / \sigma_{y0,FEM}^{PLT} \right)_{\max}$ and $\left(\sigma_{z0,FEM}^{CYL} / \sigma_{y0,FEM}^{PLT} \right)_{\min}$ is very large, Dundurs' parameters is not useful enough to discuss the ISSF of the axisymmetric bonded structure. However, the difference is less than 10% in Eq. (26); and therefore, Dundurs' parameters almost control the results and they may be useful for axisymmetric bonded structures.

Since $\left(K_{\sigma_z}^{CYL} \right)_{\max} / K_{\sigma_y}^{PLT}$ goes to infinity as $\alpha \rightarrow 2\beta$, it is not clear whether $K_{\sigma_z}^{CYL} / K_{\sigma_y}^{PLT}$ or $\sigma_{z0,FEM}^{CYL} / \sigma_{y0,FEM}^{PLT}$ is suitable for predicting the strength at present.

Useful parameter is unknown near the equal pair

$$\alpha(\alpha - 2k\beta) < 0, \quad k = 1.35 - 0.7|\beta| \quad \text{and} \quad \alpha(\alpha - 2\beta) \geq 0 \quad \text{in Fig. 8} \quad (27)$$

4. Intensity of singular stress field for bonded pipe in comparison with bonded plate

In this paper, the bonded pipe in Fig. 3(b) is also considered as another example of the most fundamental 3D bonded structures, which should be compared with the bonded plate. The schematic illustration of the bonded pipe is shown in Fig. 3(b). Here, assume that the inner radius of the pipe is infinitely large as shown in Fig. 3(b). In this case, the plain strain condition has been usually assumed. Therefore, in this paper, The ISSFs will be compared and the difference will be clarified.

Assume $L/W = 1$ and $\rho/W = 1.0 \times 10^5$ in the model. Figure 9 shows the schematic illustration of the FE mesh pattern. The same FE mesh patterns are used in all analyses. Note that the standard four-node quadrilateral plane strain elements are used for the bonded plate [7-9, 11], and similarly the standard four-node quadrilateral axisymmetric ring elements are used for the bonded pipe. Since the mesh-independent technique is used [7, 8], the singular elements such as Akin singular element are not necessary. In order to confirm the mesh dependence of the solution, the FE analyses are performed by using the coarse mesh and the fine mesh. The minimum element sizes are $e_{\min}/(W/2) = 2^{-13}$ for the coarse mesh and 2^{-17} for the fine mesh.

FEM analysis shows that $\varepsilon_{\theta 0, FEM}^{PIP} = -7.380 \times 10^{-4}$ is independent of the mesh pattern. The strain $\varepsilon_{\theta 0, FEM}^{PIP}$ causes the non-singular stresses $\tilde{\sigma}_{z0}^{PIP}$, $\left(\tilde{\sigma}_{\theta 0}^{PIP} \right)^1$, $\left(\tilde{\sigma}_{\theta 0}^{PIP} \right)^2$. Table 8 shows the FEM results of the bonded pipe in Fig. 3(b) and the bonded plate in Fig. 2. The stress ratios of the bonded pipe and the bonded plate are shown in Table 8. The singular and non-singular components are also shown in Table 8 so that the non-singular components can be confirmed at a glance. The stress ratios $\sigma_{r0, FEM}^{PIP} / \sigma_{x0, FEM}^{PLT} = \tau_{rz0, FEM}^{PIP} / \tau_{xy0, FEM}^{PLT} = 1.02$ are mesh-independent. However, the other ratios $\sigma_{\theta 0, FEM}^{PIP} / \sigma_{z0, FEM}^{PLT}$ and $\sigma_{z0, FEM}^{PIP} / \sigma_{y0, FEM}^{PLT}$ are depending on the mesh because of the non-singular stresses as mentioned in Sect. 2.1 are included in the FEM stresses.

Table 9 shows the ratios of the bonded pipe over the bonded plate by excluding the non-singular stress in

Table 8. In Table 9, all components have the same ratio 1.02 independent of the element size e_{\min} quite differently from Table 8(a).

Figure 10 shows $\sigma_{z0,FEM}^{PIP}/\sigma_{y0,FEM}^{PLT}$ and $K_{\sigma_z}^{PIP}/K_{\sigma_y}^{PLT}$ calculated by varying ν_1 from 0 to 0.5 when $(\alpha, \beta) = (0.5, 0.2)$. Here, the fine mesh pattern of $e_{\min}/(W/2) = 2^{-17}$ is used to calculate $\sigma_{z0,FEM}^{PIP}/\sigma_{y0,FEM}^{PLT}$ and $K_{\sigma_z}^{PIP}/K_{\sigma_y}^{PLT}$. Figure 10 shows that $\sigma_{z0,FEM}^{PIP}/\sigma_{y0,FEM}^{PLT}$ changes from 0.984 to 1.111 and $K_{\sigma_z}^{PIP}/K_{\sigma_y}^{PLT}$ changes from 0.953 to 1.384.

Figure 11 shows the maximum values of $K_{\sigma_z}^{PIP}/K_{\sigma_y}^{PLT}$ and $\sigma_{z0,FEM}^{PIP}/\sigma_{y0,FEM}^{PLT}$ when $\beta = 0.3$. For the bad pair $\alpha(\alpha - 2\beta) > 0$, the solid line indicates $(K_{\sigma_z}^{PIP})_{\max}/K_{\sigma_y}^{PLT}$ and the broken line indicates $(\sigma_{z0,FEM}^{PIP}/\sigma_{y0,FEM}^{PLT})_{\max}$. For the good pair $\alpha(\alpha - 2\beta) < 0$, the solid line indicates the $(\sigma_{z0,FEM}^{PIP}/\sigma_{y0,FEM}^{PLT})_{\max}$ and for the equal pair $\alpha(\alpha - 2\beta) = 0$, the open circle mark indicates $(\sigma_{z0,FEM}^{PIP}/\sigma_{y0,FEM}^{PLT})_{\max}$. When $\alpha(\alpha - 2\beta) > 0$, $(K_{\sigma_z}^{PIP})_{\max}/K_{\sigma_y}^{PLT}$ may be useful for predicting the debonding strength since the singular stress appears. On the other hand, when $\alpha(\alpha - 2\beta) \leq 0$, $(\sigma_{z0,FEM}^{PIP}/\sigma_{y0,FEM}^{PLT})_{\max}$ may be useful since there is no singular stress.

Figure 12 and Tables 10, 11 show the maximum values and the minimum values of $K_{\sigma_z}^{PIP}/K_{\sigma_y}^{PLT}$ and $\sigma_{z0,FEM}^{PIP}/\sigma_{y0,FEM}^{PLT}$ calculated by varying (α, β) . When $\alpha(\alpha - 2\beta) > 0$, the ISSF ratio $K_{\sigma_z}^{PIP}/K_{\sigma_y}^{PLT}$ may be useful predicting the debonding strength. When $\alpha(\alpha - 2\beta) \leq 0$, the stress ratio $\sigma_{z0,FEM}^{PIP}/\sigma_{y0,FEM}^{PLT}$ may be important for predicting the debonding strength. However, when $\alpha \cong 2\beta$, it is not clear whether $K_{\sigma_z}^{PIP}/K_{\sigma_y}^{PLT}$ or $\sigma_{z0,FEM}^{PIP}/\sigma_{y0,FEM}^{PLT}$ is suitable for predicting the strength at present because $(K_{\sigma_z}^{PIP})_{\max}/K_{\sigma_y}^{PLT}$ goes to ∞ as $\alpha \rightarrow 2\beta$.

As shown in Table 10, for most cases, $(K_{\sigma_z}^{PIP})_{\max}/K_{\sigma_y}^{PLT}$ value is larger than 1. This is the reason why $K_{\sigma_z}^{PIP}$ does not correspond to the $K_{\sigma_y}^{PLT}$ even in the case $\rho \rightarrow \infty$. Table 10 shows that the bonded pipe is more severe than the bonded plate mechanically. Although the ISSF ratio $(K_{\sigma_z}^{PIP})_{\max}/K_{\sigma_y}^{PLT}$ goes to ∞ under the equal pair, $(K_{\sigma_z}^{PIP})_{\max}/K_{\sigma_y}^{PLT}$ is less than about 1.5 in the region $\alpha(\alpha - 2k\beta) \geq 0$, $k = 1.3 - 0.6|\beta|$.

$$\frac{(K_{\sigma_z}^{PIP})_{\max}}{K_{\sigma_y}^{PLT}} \leq 1.5 \quad \text{for most of the bad pair } \alpha(\alpha - 2k\beta) \geq 0, \quad k = 1.3 - 0.6|\beta| \quad \text{in Fig. 8} \quad (28)$$

As shown in Fig. 8, the bonded pipe ISSF ratio satisfies < 1.5 in the wider range of the bonded cylinder. This is because the bonded pipe is much closer to the bonded plate compared to the bonded cylinder. The stress ratio $(\sigma_{z0,FEM}^{PIP}/\sigma_{y0,FEM}^{PLT})_{\max}$ does not diverge. Comparing Fig. 12(a) with Fig. 12(b), it is found that the value of $\sigma_{z0,FEM}^{PIP}/\sigma_{y0,FEM}^{PLT}$ varies depending on (α, β) . For all of the good pair $\alpha(\alpha - 2\beta) < 0$, the range of $(\sigma_{z0,FEM}^{PIP}/\sigma_{y0,FEM}^{PLT})_{\max}$ is not very large and the difference between $(\sigma_{z0,FEM}^{PIP}/\sigma_{y0,FEM}^{PLT})_{\max}$ and $(\sigma_{z0,FEM}^{PIP}/\sigma_{y0,FEM}^{PLT})_{\min}$ is in the following region.

$$1.0 \leq \left(\frac{\sigma_{z0,FEM}^{PIP}}{\sigma_{y0,FEM}^{PLT}} \right)_{\max} \leq 1.4, \quad \frac{\left(\frac{\sigma_{z0,FEM}^{PIP}}{\sigma_{y0,FEM}^{PLT}} \right)_{\max} - \left(\frac{\sigma_{z0,FEM}^{PIP}}{\sigma_{y0,FEM}^{PLT}} \right)_{\min}}{\left(\frac{\sigma_{z0,FEM}^{PIP}}{\sigma_{y0,FEM}^{PLT}} \right)_{\max} + \left(\frac{\sigma_{z0,FEM}^{PIP}}{\sigma_{y0,FEM}^{PLT}} \right)_{\min}} \leq 0.105 \quad (29)$$

for all of the good pair $\alpha(\alpha - 2\beta) < 0$ in Fig. 8

As shown in Eq. (29), since the difference between $(\sigma_{z0,FEM}^{PIP}/\sigma_{y0,FEM}^{PLT})_{\max}$ and $(\sigma_{z0,FEM}^{PIP}/\sigma_{y0,FEM}^{PLT})_{\min}$ is small enough, Dundurs' parameters (α, β) is suitable for expressing the interface stress of the bonded pipe. FEM stress ratio of

the bonded pipe is smaller than that of the bonded cylinder. From Figs 7, 12 and Tables 6, 7, 10, 11, it may be concluded that the ISSF of the bonded cylinder is more severe than the ISSF of the bonded pipe in all material combination.

Since the ratio $(K_{\sigma_z}^{PIP})_{\max}/K_{\sigma_y}^{PLT}$ goes to ∞ as $\alpha \rightarrow 2\beta$, it is not clear whether $K_{\sigma_z}^{PIP}/K_{\sigma_y}^{PLT}$ or $\sigma_{z0,FEM}^{PIP}/\sigma_{y0,FEM}^{PLT}$ is suitable for predicting of the strength is not clarified in the following range at present.

Useful parameter is unknown near the equal pair

$$\alpha(\alpha - 2k\beta) < 0, \quad k = 1.3 - 0.6|\beta| \quad \text{and} \quad \alpha(\alpha - 2\beta) \geq 0 \quad \text{in Fig. 8} \quad (30)$$

5. Conclusion

The authors have shown that the bonded strength can be expressed as a constant value of the ISSF assuming two dimensional modelling [9-11]. Since real structures always have three dimensional geometries, in this paper, the most fundamental bonded problems were considered. From the comparison among the bonded cylinder ($K_{\sigma_z}^{CYL}$, $\sigma_{z0,FEM}^{CYL}$), the bonded pipe ($K_{\sigma_z}^{PIP}$, $\sigma_{z0,FEM}^{PIP}$) and the bonded plate ($K_{\sigma_y}^{PLT}$, $\sigma_{y0,FEM}^{PLT}$), the following conclusion can be drawn. Here, $K_{\sigma_z}^{CYL}$, $K_{\sigma_z}^{PIP}$, $K_{\sigma_y}^{PLT}$ are ISSFs and $\sigma_{z0,FEM}^{CYL}$, $\sigma_{z0,FEM}^{PIP}$, $\sigma_{y0,FEM}^{PLT}$ are the stress at the interface end.

1. The maximum and minimum values of $K_{\sigma_z}^{CYL}/K_{\sigma_y}^{PLT}$ and $\sigma_{z0,FEM}^{CYL}/\sigma_{y0,FEM}^{PLT}$ of the bonded cylinder were shown in the charts and tables. For most of the bad pair satisfying $\alpha\{\alpha - (2.7 - 1.4|\beta|)\beta\} \geq 0$ in Fig. 8, it was

found that the ISSF ratio $(K_{\sigma_z}^{CYL})_{\max}/K_{\sigma_y}^{PLT} \leq 1.5$. For most of the good pair $0 \leq |\beta| \leq 0.3$ and $\alpha(\alpha - 2\beta) < 0$,

the stress ratio satisfies $1.0 \leq (\sigma_{z0,FEM}^{CYL}/\sigma_{y0,FEM}^{PLT})_{\max} \leq 1.5$. It was found that the difference between $(\sigma_{z0,FEM}^{CYL}/\sigma_{y0,FEM}^{PLT})_{\max}$ and $(\sigma_{z0,FEM}^{CYL}/\sigma_{y0,FEM}^{PLT})_{\min}$ is less than about 10%; and therefore, Dundurs' parameters almost control the results and they may be useful for axisymmetric bonded structures.

2. The maximum and minimum values of $K_{\sigma_z}^{PIP}/K_{\sigma_y}^{PLT}$ and $\sigma_{z0,FEM}^{PIP}/\sigma_{y0,FEM}^{PLT}$ of the bonded pipe were shown in the charts and tables when the pipe inner radius $\rho \rightarrow \infty$. The results of the bonded pipe do not coincide with the ones of the bonded plate completely even when $\rho \rightarrow \infty$. For most of the bad pairs satisfying

$\alpha\{\alpha - (2.6 - 1.2|\beta|)\beta\} \geq 0$ in Fig. 8, the ISSF ratio $(K_{\sigma_z}^{PIP})_{\max}/K_{\sigma_y}^{PLT} \leq 1.5$. As shown in Fig.8, the bonded pipe

ISSF ratio satisfies < 1.5 in the wider range of the bonded cylinder. This is because the bonded pipe is more closer to the bonded plate compared to the bonded cylinder. For all of the good pair $\alpha(\alpha - 2\beta) < 0$, the stress ratio is in the region $1.0 \leq (\sigma_{z0,FEM}^{PIP}/\sigma_{y0,FEM}^{PLT})_{\max} \leq 1.4$. The differences between $(\sigma_{z0,FEM}^{PIP}/\sigma_{y0,FEM}^{PLT})_{\max}$ and $(\sigma_{z0,FEM}^{PIP}/\sigma_{y0,FEM}^{PLT})_{\min}$ were less than about 10%. The stress ratio of the bonded pipe is smaller than that of the bonded cylinder. It was found that the ISSF of the bonded cylinder is more severe than the ISSF of the bonded pipe in all material combination.

3. For the bad pair $\alpha(\alpha - 2\beta) > 0$, the ISSF ratio $K_{\sigma_z}^{CYL}/K_{\sigma_y}^{PLT}$ and $K_{\sigma_z}^{PIP}/K_{\sigma_y}^{PLT}$ may be useful for evaluating the debonding strength since the singular stress appears. For good pair $\alpha(\alpha - 2\beta) < 0$, the stress ratio $\sigma_{z0,FEM}^{CYL}/\sigma_{y0,FEM}^{PLT}$ and $\sigma_{z0,FEM}^{PIP}/\sigma_{y0,FEM}^{PLT}$ may be useful although equal pair region $\alpha \cong 2\beta$, useful parameter is not known. It was found that $(K_{\sigma_z}^{CYL})_{\max}/K_{\sigma_y}^{PLT} \rightarrow \infty$ as $\alpha \rightarrow 2\beta$. However, as shown in Fig. 6(b), the

singular stress field disappears since the index $\lambda \rightarrow 1$ as $\alpha \rightarrow 2\beta$. The future experimental study may be necessary to confirm the usefulness of those results.

4. It was found that the mesh-independent technique is useful for analyzing the bonded cylinder and the bonded pipe by subtracting the non-singular stress from FEM stresses. In the FE analysis, it was found that the non-singular stresses caused by the circumferential strain are contained in the FEM stresses at the interface end. The non-singular stresses were derived from the boundary conditions explicitly.

References

1. Barnes, T. A., Pashby, I. R., Joining techniques for aluminium spaceframes used in automobiles: Part II - adhesive bonding and mechanical fasteners, *Journal of Materials Processing Technology*, Vol. 99 (2000), pp. 72 - 79.
2. Higgins, A., Adhesive bonding of aircraft structures, *International Journal of Adhesion and Adhesives*, Vol. 20, No. 5 (2000), pp. 367 - 376.
3. Petrie, E. M., Adhesives for the assembly of aircraft structures and components: Decades of performance improvement, with the new applications of the horizon, *Metal Finishing*, Vol. 106, No. 2 (2008), pp. 26 - 31.
4. Qian, Z., Akisanya, A. R., An experimental investigation of failure initiation in bonded joints, *Acta Materialia*, Vol. 46, No. 14 (1998), pp. 4895 - 4904.
5. Akisanya, A. R., Meng, C. S., Initiation of fracture at the interface corner of bi-material joints, *Journal of the Mechanics and Physics of Solids*, Vol. 51 (2003), pp. 27 - 46.
6. Mintzas, A., Nowell, D., Validation of an H_{cr} -based fracture initiation criterion for adhesively bonded joints, *Engineering Fracture Mechanics*, Vol. 80 (2012), pp. 13 - 27.
7. Zhang, Y., Noda, N. -A., Wu, P. and Duan, M., A mesh-independent technique to evaluate stress singularities in adhesive joints, *International Journal of Adhesion and adhesives*, Vol. 57 (2015), pp. 105 - 117.
8. Zhang, Y., Noda, N. -A., Wu, P. and Duan, M., Corrigendum to “A mesh-independent technique to evaluate stress singularities in adhesive joints [International Journal of Adhesion and adhesives, Vol. 57 (2015), pp. 105 - 117]”, *International Journal of Adhesion and adhesives*, Vol. 60 (2015), pp. 130.
9. Miyazaki, T., Noda, N. -A., Li, R., Uchikoba, T., Sano, Y., Debonding criterion for single lap joints from the intensity of singular stress field, *Journal of the Japan Institute of Electronics Packaging*, Vol. 16, No. 2 (2013), pp. 143 - 151 (in Japanese).
10. Miyazaki, T., Noda, N. -A., Uchikoba, T., Li, R., Sano, Y., Proposal of a Convenient and Accurate Method for Evaluation of Debonding Strength, *Transactions of the Society of Automative Engineers of Japan*, Vol. 45, No. 5 (2014), pp. 895 - 901 (in Japanese).
11. Noda, N. -A., Miyazaki, T., Uchikoba, T., Li, R., Sano, Y., Takase, Y., Debonding strength evaluation in terms of the intensity of singular stress at the interface corner with and without fictitious crack, *International Journal of Adhesion and Adhesives*, Vol. 61 (2015), pp. 46 - 64.
12. Noda, N., Tsuji, T., Stress singularities in edge-bonded dissimilar wedges : Three dimensional axisymmetrical elastic problems, *Transactions of the Japan Society of Mechanical Engineers, Series A*, Vol. 58, No. 546 (1992), pp. 275 - 278 (in Japanese).

13. Hu, Q., Sato, Y., Watanabe, K., Dependence of stress state on elastic constants in axisymmetric dissimilar materials, Transactions of the Japan Society of Mechanical Engineers, Series A, Vol. 65, No. 633 (1999), pp. 1010 - 1017 (in Japanese).
14. Hu, Q., Watanabe, K., A study on fundamental properties of elastic parameters related to stress field for dissimilar materials, Transactions of the Japan Society of Mechanical Engineers, Series A, Vol. 69, No. 679 (2003), pp. 594 - 601 (in Japanese).
15. Li, Y. L., Hu, S. Y., Munz, D., Yang, Y. Y., Asymptotic description of the stress field around the bond edge of a cylindrical joint, Archive of Applied Mechanics, Vol. 68, No. 7 - 8 (1998), pp. 552 - 565.
16. Dundurs, J., Discussion of edge-bonded dissimilar orthotropic elastic wedges under normal and shear loading, Transaction of the ASME, Journal of Applied Mechanics, Vol. 36 (1969), pp. 650 - 652.
17. Bogy, D. B., Edge-bonded dissimilar orthogonal elastic wedges under normal and shear loading, Transaction of the ASME, Journal of Applied Mechanics, Vol. 35 (1968), pp. 460 - 466.
18. Bogy, D. B., Two edge-bonded elastic wedges of different and wedge angles under surface tractions, Transaction of the ASME, Journal of Applied Mechanics, Vol. 38 (1971), pp. 377 - 386.
19. Yuuki, R., Xu, J. -Q, Liu, J. -Q., Analysis of Stress Singularity at Interface Edge in Dissimilar Materials, Seisan Kenkyu, Vol. 44, No. 4 (1992), pp. 206 - 210 (in Japanese).
20. Timoshenko, S. P., Goodier, J. N., Theory of Elasticity, Third Edition (1970), pp. 380, McGraw-Hill, New York.
21. Noda, N. -A., Shirao, R., Li, J., Sugimoto, J. -S, Intensity of singular stress fields causing interfacial debonding at the end of a fiber under pullout force and transverse tension, International Journal of Solids and Structures, Vol. 44, No. 13 (2007), pp. 4472 - 4491.
22. Carpenter, W. C., Byers, C., A path independent integral for computing stress intensities for V-notched cracks in a bi-material, International Journal of Fracture, Vol. 35 (1978), pp. 245 - 268.
23. Naito, K., Onta, M. and Kogo, Y., The effect of adhesive thickness on tensile and shear strength of polyimide adhesive, International Journal of Adhesion and Adhesives, Vol. 36 (2012), pp. 77 - 85.

Appendix A: Debonding strength evaluation for cylindrical butt joint

In this paper, the ISSF for the bonded cylinder and the bonded pipe was discussed under arbitrary material combination. To clarify the usefulness of the present results, the debonding strength of the cylindrical butt joints is discussed by using experiment of Naito et al [23]. Figure A1 shows the schematic illustration of the specimens. In the experiment, the adherend and adhesive are aluminum alloy 5052-H34 (Young's modulus $E_1 = 69.6$ GPa, Poisson's ratio $\nu_1 = 0.33$) and polyimide adhesive ($E_2 = 3.77$ GPa, $\nu_2 = 0.342$), respectively. Table A1 shows Dundurs' parameters (α, β) and singular index λ . The length of the adherend, l , is 38.1 mm; the adhesive thickness t is varied from 0.2 mm to 0.6 mm. Figure A2 shows the experimentally obtained tensile strength. Here, the debonding crack was initiated from the end of the interface between the adhesive and the adherend. The tensile strength σ_f increases with increasing the adhesive thickness.

The cylindrical butt joint in Fig. A1 was analyzed by applying the same analytical method. Figure A3 shows the dimensionless ISSF, $F_{\sigma_z}^{CBJ} = K_{\sigma_z}^{CBJ} / (\sigma_z^\infty d^{1-\lambda})$ for Fig. A1. The $F_{\sigma_z}^{CBJ}$ value increases with increasing the

adhesive thickness t and coincides with the value in Fig. 7 and Table 6. Figure A4 shows the critical value of $K_{\sigma_z}^{CBJ}$ defined as $K_{\sigma_c}^{CBJ} = K_{\sigma_z}^{CBJ} \Big|_{\sigma_z^c = \sigma_f}$. It is seen that the $K_{\sigma_c}^{CBJ}$ values are almost constant independent of the adhesive thickness. It is confirmed that the ISSF is useful for evaluating the debonding strength.

Figure contents

- Fig. 1 Schematic illustration of butt joint
- Fig. 2 Schematic illustration of bonded plate
- Fig. 3 Schematic illustration of bonded cylinder and bonded pipe
- Fig. 4 FE mesh pattern used in analyses of bonded cylinder and bonded plate
- Fig. 5 Variation of elastic parameters E_2/E_1 and ν_2 under fixed $(\alpha, \beta) = (0.8, 0.3)$ and variations of stress ratio $\sigma_{z0,FEM}^{CYL} / \sigma_{y0,FEM}^{PLT}$ and ISSF ratio $K_{\sigma_z}^{CYL} / K_{\sigma_y}^{PLT}$ under fixed $(\alpha, \beta) = (0.8, 0.3)$
- (a) E_2/E_1 vs ν_1
- (b) ν_2 vs ν_1
- (c) $K_{\sigma_z}^{CYL} / K_{\sigma_y}^{PLT}$ and $\sigma_{z0,FEM}^{CYL} / \sigma_{y0,FEM}^{PLT}$ vs ν_1
- Fig. 6 Maximum values of $K_{\sigma_z}^{CYL} / K_{\sigma_y}^{PLT}$ and $\sigma_{z0,FEM}^{CYL} / \sigma_{y0,FEM}^{PLT}$ when $\beta = 0.3$
- (a) Maximum values of $K_{\sigma_z}^{CYL} / K_{\sigma_y}^{PLT}$ and $\sigma_{z0,FEM}^{CYL} / \sigma_{y0,FEM}^{PLT}$
- (b) λ
- (c) $F_{\sigma_y}^{PLT}$
- Fig. 7 $K_{\sigma_z}^{CYL} / K_{\sigma_y}^{PLT}$ and $\sigma_{z0,FEM}^{CYL} / \sigma_{y0,FEM}^{PLT}$ in (α, β) map
- (a) Maximum values
- (b) Minimum values
- Fig. 8 Dundurs' parameters for several engineering materials
- Fig. 9 FE mesh pattern used in analyses of bonded pipe and bonded plate
- Fig. 10 $\sigma_{z0,FEM}^{PIP} / \sigma_{y0,FEM}^{PLT}$ and $K_{\sigma_z}^{PIP} / K_{\sigma_y}^{PLT}$ values depending on ν_1 when (α, β) is fixed as $(0.5, 0.2)$
- Fig. 11 Maximum values of $K_{\sigma_z}^{PIP} / K_{\sigma_y}^{PLT}$ and $\sigma_{z0,FEM}^{PIP} / \sigma_{y0,FEM}^{PLT}$ when $\beta = 0.3$
- Fig. 12 $K_{\sigma_z}^{PIP} / K_{\sigma_y}^{PLT}$ and $\sigma_{z0,FEM}^{PIP} / \sigma_{y0,FEM}^{PLT}$ in (α, β) map
- (a) Maximum values
- (b) Minimum values
- Fig. A1 Schematic illustration of cylindrical butt joint
- Fig. A2 Relation between the tensile strength σ_f and adhesive thickness t
- Fig. A3 Dimensionless ISSF for the cylindrical butt joint, $F_{\sigma_z}^{CBJ}$
- Fig. A4 The critical ISSF, $K_{\sigma_c}^{CBJ}$

Table contents

Table 1	An example of bad pair $(\alpha, \beta) = (0.8, 0.3)$ satisfying $\alpha(\alpha - 2\beta) > 0$ used to explain the present analysis
Table 2	Mesh-dependent FEM stress/strain at the interface end when $(\alpha, \beta) = (0.8, 0.3)$ and $\nu_1 = 0.2555$ in Table 1
	(a) Bonded cylinder (Mesh-dependent except for ε_θ)
	(b) Bonded plate (Mesh-dependent except for ε_z)
Table 3	Mesh-independent $\varepsilon_{\theta 0, FEM}^{CYL}$ values obtained by $u_{r0, FEM}^{CYL}$ and $\sigma_{j0, FEM}^{CYL}$ (=singular strain + non-singular strain) when $(\alpha, \beta) = (0.8, 0.3)$ and $\nu_1 = 0.2555$ in Table 1
Table 4	FEM stress ratio for the bonded cylinder when $(\alpha, \beta) = (0.8, 0.3)$ and $\nu_1 = 0.2555$ in Table 1 [= (singular stress + non-singular stress) / singular stress] (See Sect. 2.3)
	(a) Bonded cylinder / bonded plate (Mesh-independent if non-singular stress is zero)
	(b) Butt joint / bonded plate (Mesh-independent because non-singular stress is always zero)
	(c) FEM stress of butt joint [= singular stress + non-singular stress (= 0)] (Mesh-dependent)
Table 5	FEM stress ratio by excluding non-singular stress (a) as shown in Table 5(c) when $(\alpha, \beta) = (0.8, 0.3)$ and $\nu_1 = 0.2555$ in Table 1
	(a) Non-singular FEM stress of the bonded cylinder obtained by using explicit Eqs. (14), (15), (18), (19), (20) (Mesh-independent)
	(b) Singular FEM stress of the bonded cylinder by excluding non-singular stress in Table 5 (a) (Mesh-dependent)
	(c) FEM stress ratio of the bonded cylinder over the bonded plate (Mesh-independent quite differently from Table 4(a) by excluding the non-singular stress in Table 5 (a))
	(d) Dimensionless ISSFs in Eq. (21) and Eq. (22) obtained from the unique ratio in Table 5 (c)
	(e) Mesh-independent FEM stress ratio also independent of distance R in Fig. 2 and Fig. 3
Table 6	Maximum and minimum values of $K_{\sigma_z}^{CYL} / K_{\sigma_y}^{PLT}$
Table 7	Maximum and minimum values of $\sigma_{z0, FEM}^{CYL} / \sigma_{y0, FEM}^{PLT}$
Table 8	FEM stress ratio for the bonded pipe when $(\alpha, \beta) = (0.8, 0.3)$ and $\nu_1 = 0.2555$ in Table 1 [= (singular stress + non-singular stress) / singular stress]
	(a) Bonded pipe / bonded plate (Mesh-independent if non-singular stress is zero)
	(b) FEM stress of bonded pipe (Mesh-dependent) [= singular stress + non-singular stress]
	(c) FEM stress of bonded plate (Mesh-dependent) [= singular stress + non-singular stress (= 0)]
Table 9	FEM stress ratio of the bonded cylinder over the bonded plate (Mesh-independent differently from Table 8(a) by excluding the non-singular stress)
Table 10	Maximum and minimum values of $K_{\sigma_z}^{PIP} / K_{\sigma_y}^{PLT}$
Table 11	Maximum and minimum values of $\sigma_{z0, FEM}^{PIP} / \sigma_{y0, FEM}^{PLT}$
Table A1	Dundurs' parameters (α, β) and singular index λ

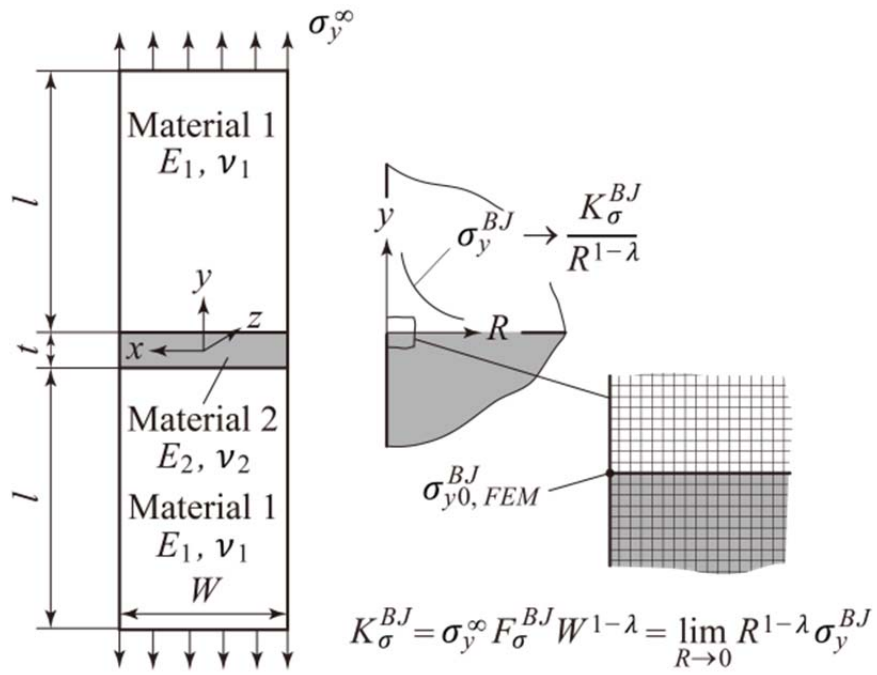


Fig. 1 Schematic illustration of butt joint

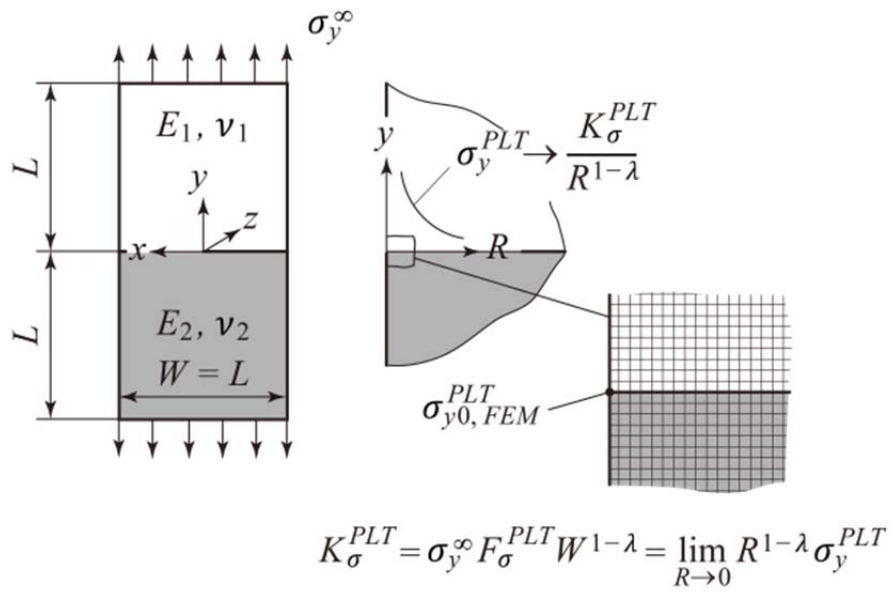
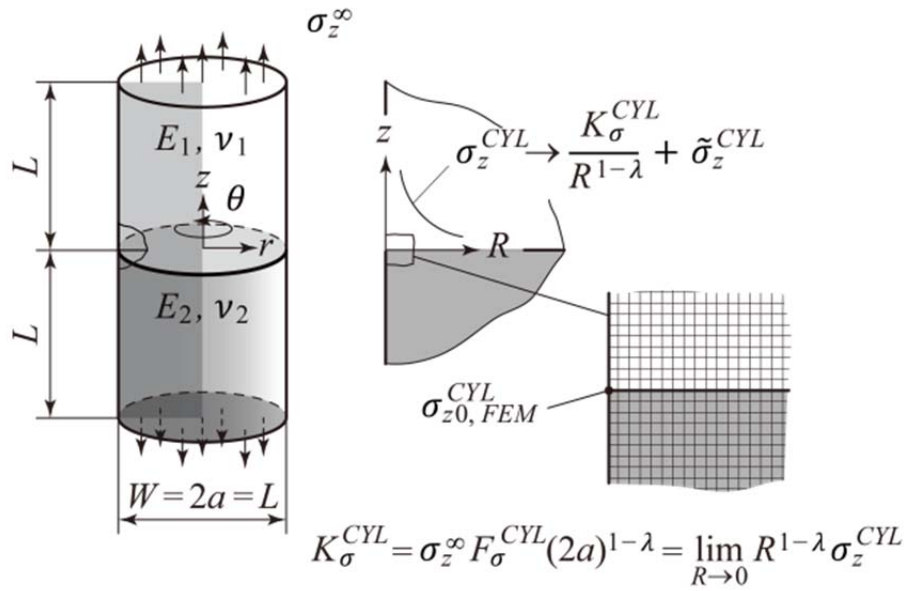
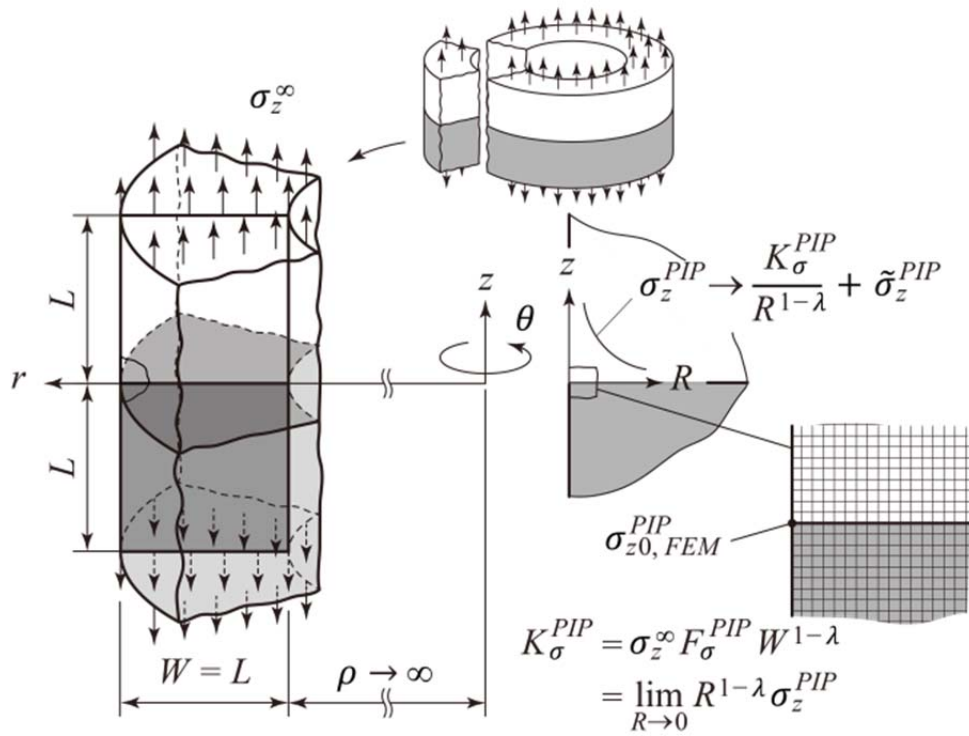


Fig. 2 Schematic illustration of bonded plate



(a) Bonded cylinder



(b) Bonded pipe

Fig. 3 Schematic illustration of bonded cylinder and bonded pipe

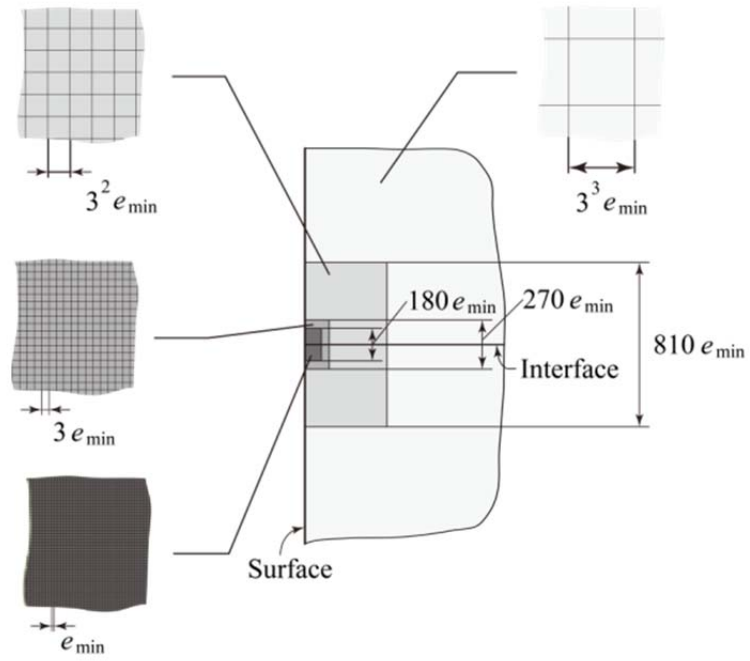
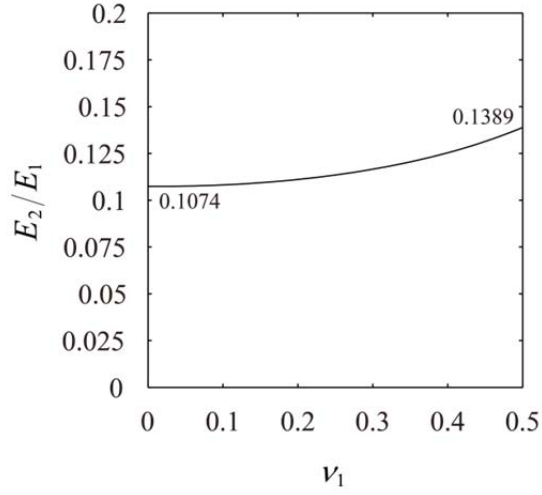
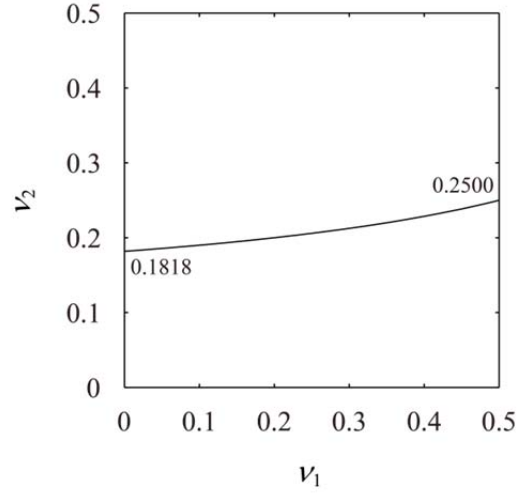


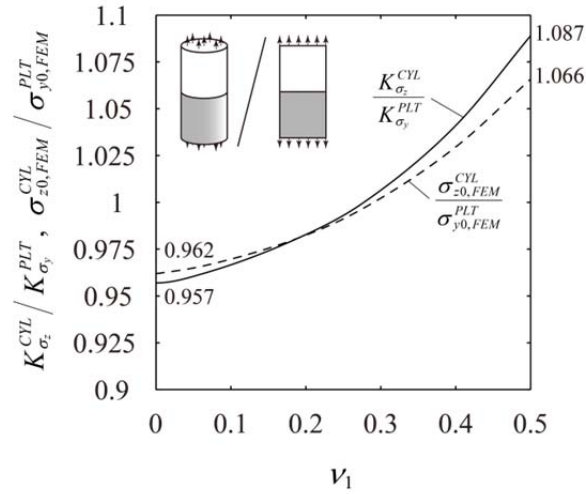
Fig. 4 FE mesh pattern used in analyses of bonded cylinder and bonded plate



(a) E_2/E_1 vs ν_1

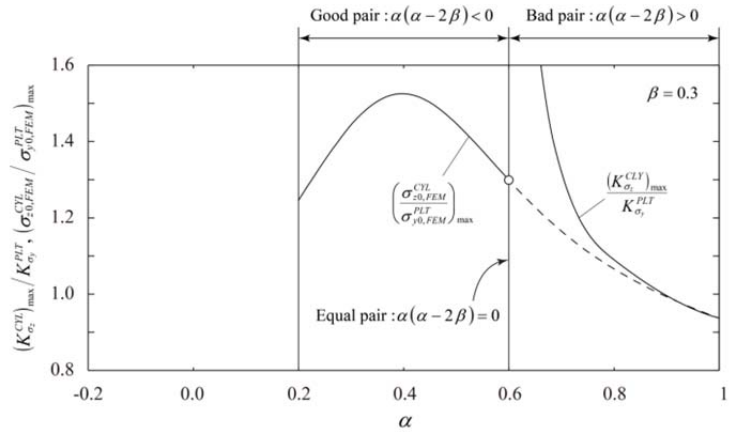


(b) ν_2 vs ν_1

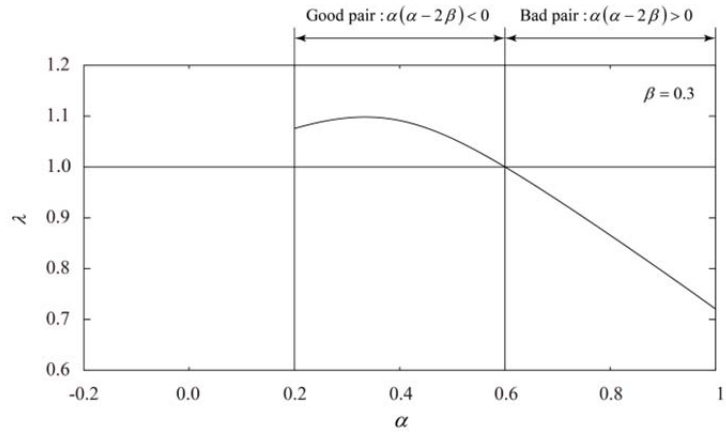


(c) $K_{\sigma_z}^{CYL}/K_{\sigma_y}^{PLT}$ and $\sigma_{z0,FEM}^{CYL}/\sigma_{y0,FEM}^{PLT}$ vs ν_1

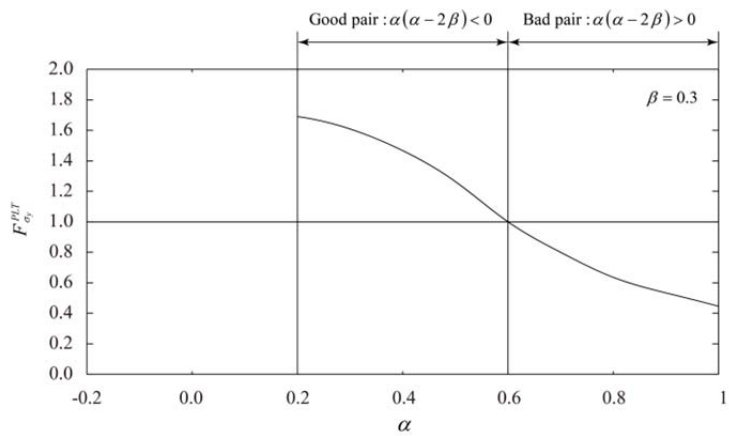
Fig. 5 Variation of elastic parameters E_2/E_1 and ν_2 under fixed $(\alpha, \beta) = (0.8, 0.3)$ and variations of stress ratio $\sigma_{z0,FEM}^{CYL}/\sigma_{y0,FEM}^{PLT}$ and ISSF ratio $K_{\sigma_z}^{CYL}/K_{\sigma_y}^{PLT}$ under fixed $(\alpha, \beta) = (0.8, 0.3)$



(a) Maximum values of $K_{\sigma_z}^{CYL}/K_{\sigma_y}^{PLT}$ and $\sigma_{z0,FEM}^{CYL}/\sigma_{y0,FEM}^{PLT}$

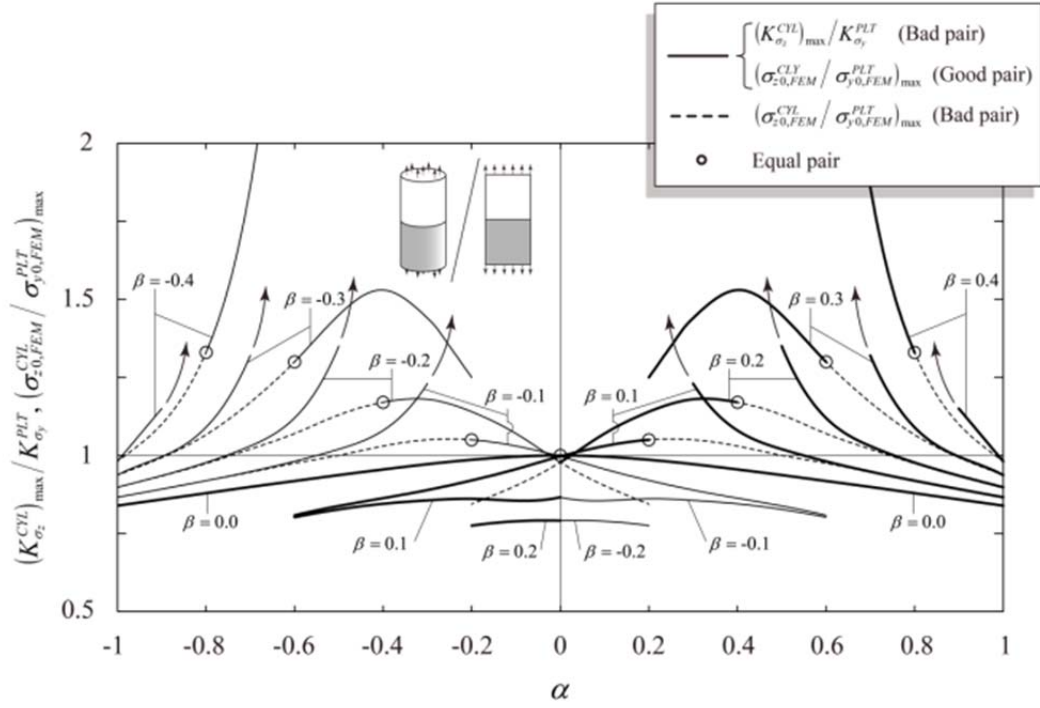


(b) λ

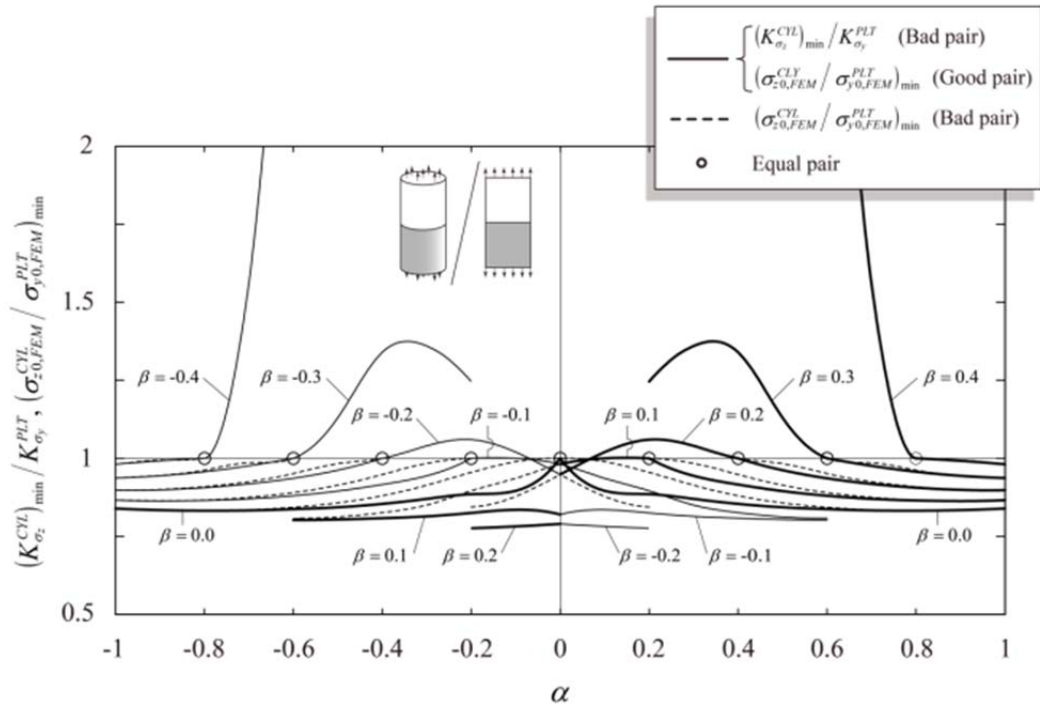


(c) $F_{\sigma_y}^{PLT}$

Fig. 6 Maximum values of $K_{\sigma_z}^{CYL}/K_{\sigma_y}^{PLT}$ and $\sigma_{z0,FEM}^{CYL}/\sigma_{y0,FEM}^{PLT}$ when $\beta = 0.3$



(a) Maximum values



(b) Minimum values

Fig. 7 $K_{\sigma_z}^{CYL} / K_{\sigma_y}^{PLT}$ and $\sigma_{z,0,FEM}^{CYL} / \sigma_{y,0,FEM}^{PLT}$ in (α, β) map

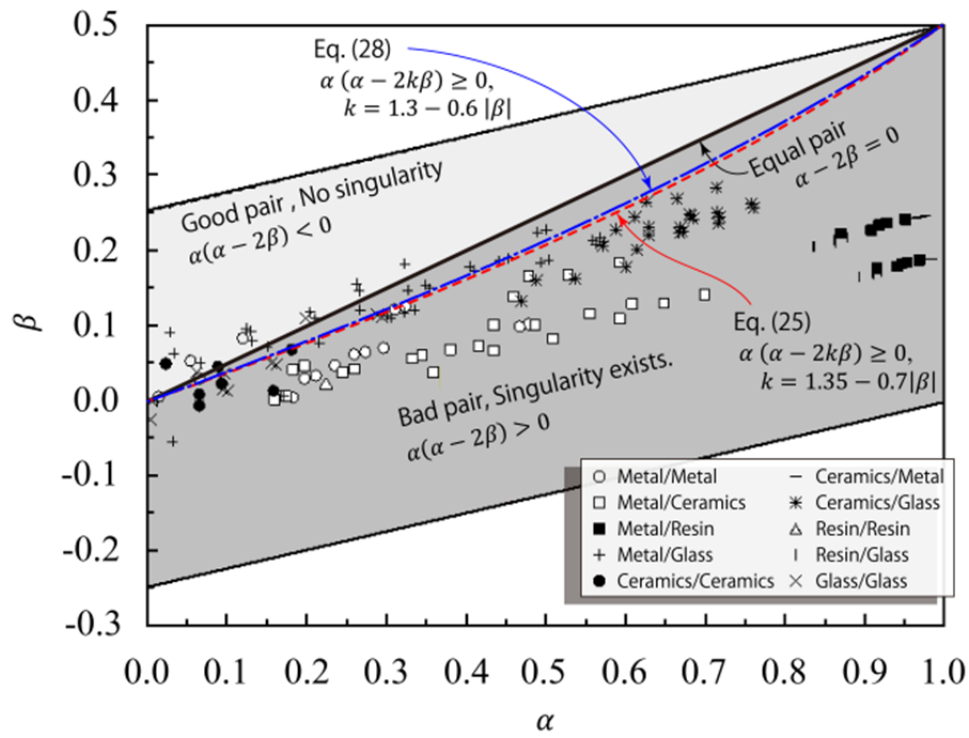


Fig. 8 Dundurs' parameters for several engineering materials

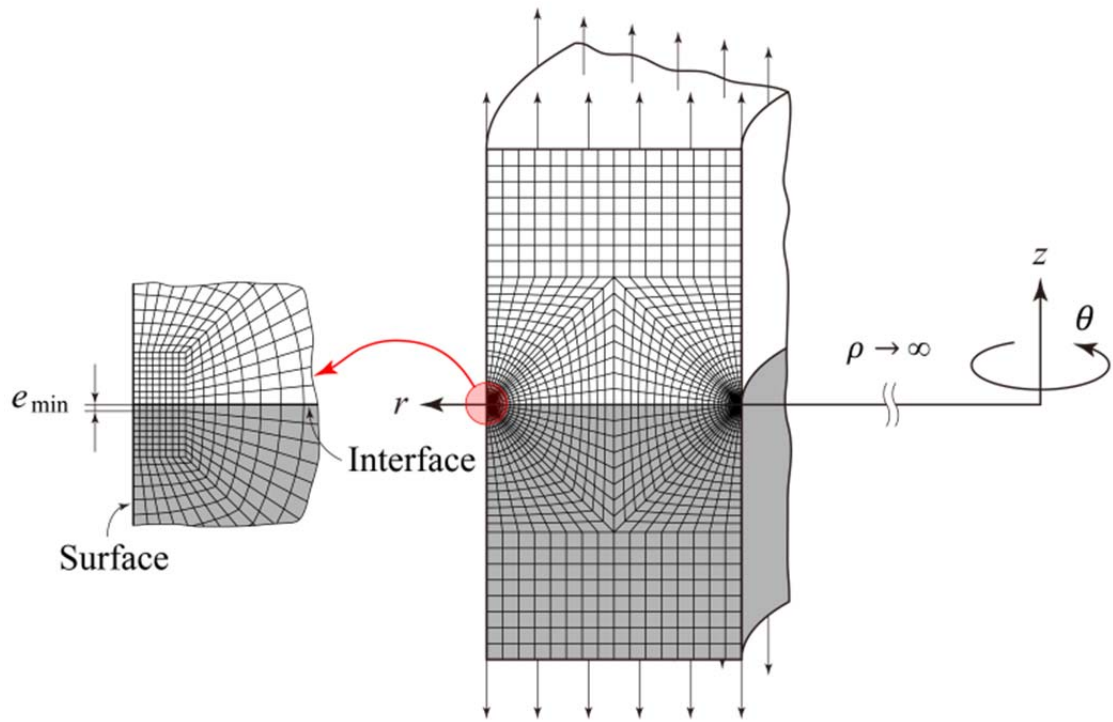


Fig. 9 FE mesh pattern used in analyses of bonded pipe and bonded plate

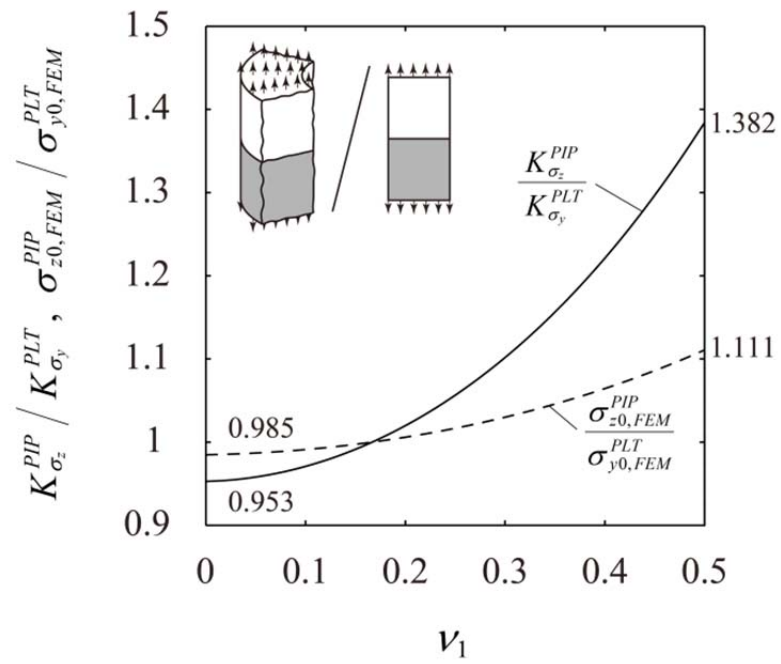


Fig. 10 $\sigma_{z0,FEM}^{PIP} / \sigma_{y0,FEM}^{PLT}$ and $K_{\sigma_z}^{PIP} / K_{\sigma_y}^{PLT}$ values depending on ν_1 when (α, β) is fixed as $(0.5, 0.2)$

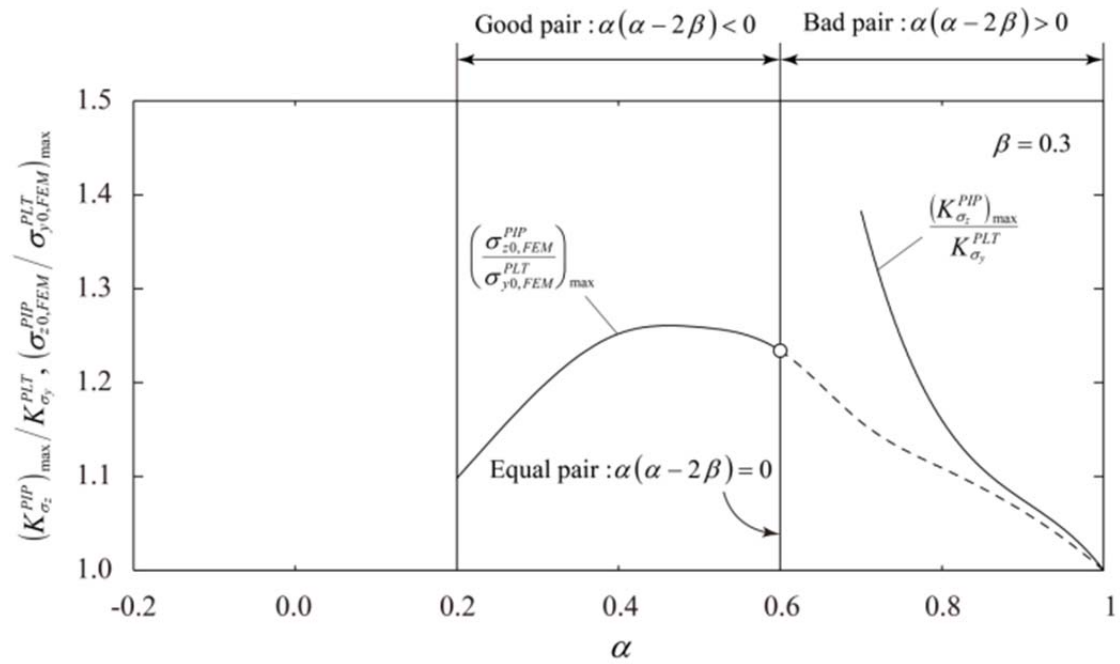
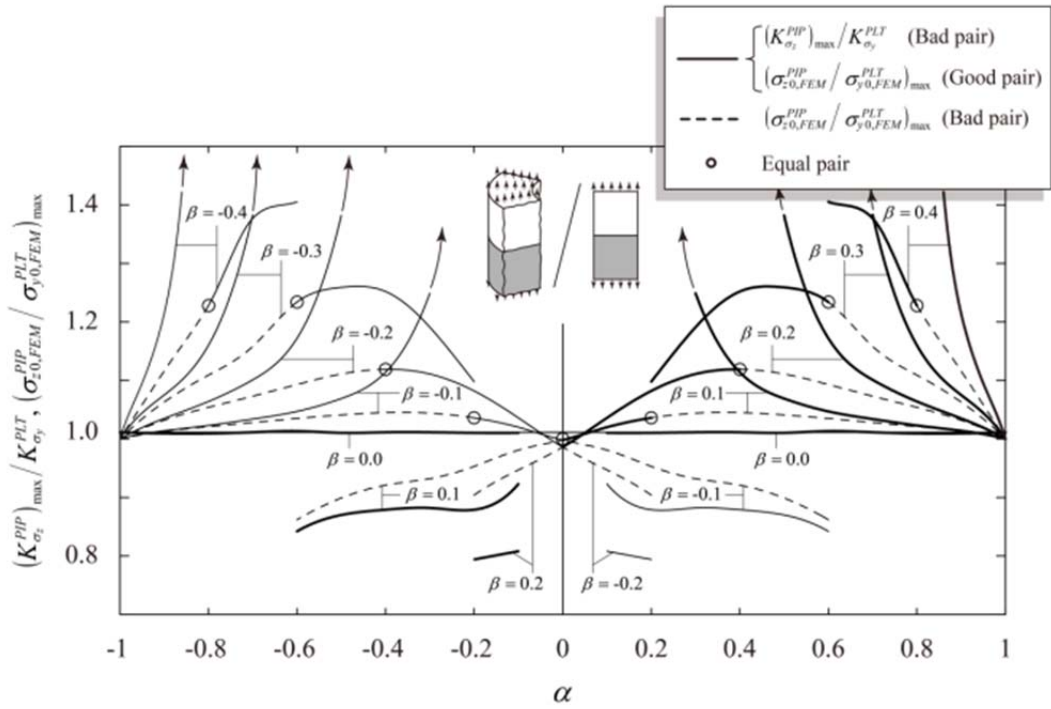
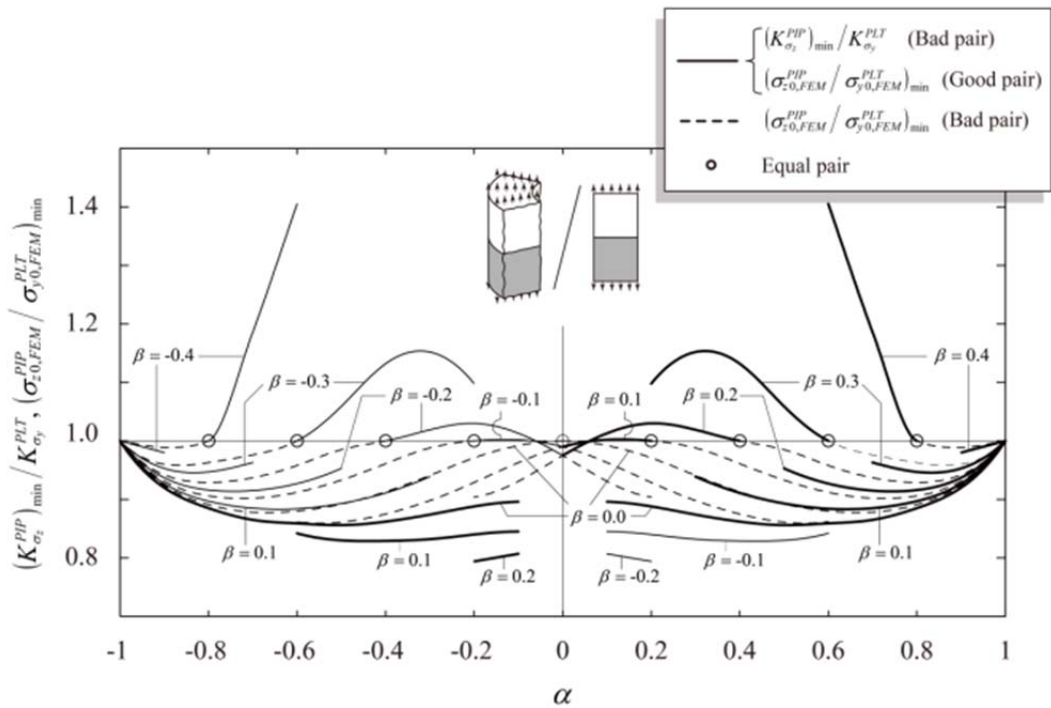


Fig. 11 Maximum values of $K_{\sigma_z}^{PIP} / K_{\sigma_y}^{PLT}$ and $\sigma_{z0,FEM}^{PIP} / \sigma_{y0,FEM}^{PLT}$ when $\beta = 0.3$



(a) Maximum values



(b) Minimum values

Fig. 12 $K_{\sigma_z}^{PIP} / K_{\sigma_z}^{PLT}$ and $\sigma_{z,0,FEM}^{PIP} / \sigma_{y,0,FEM}^{PLT}$ in (α, β) map

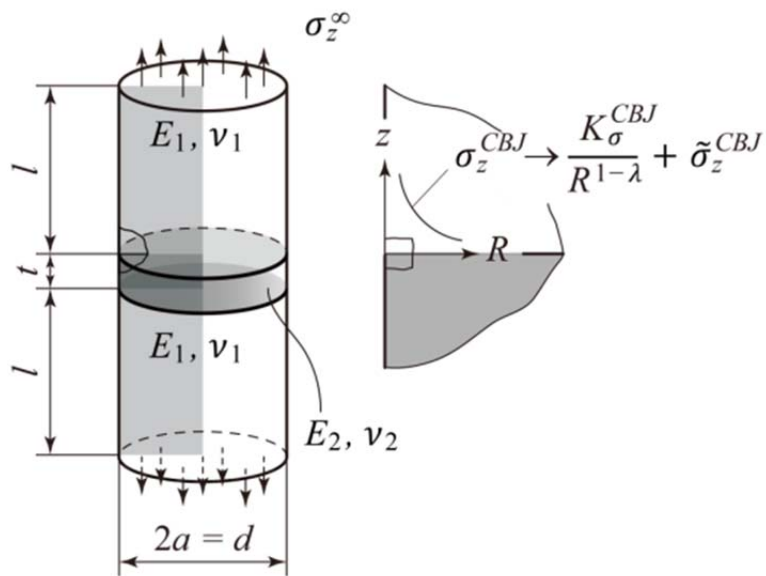


Fig. A1 Schematic illustration of cylindrical butt joint

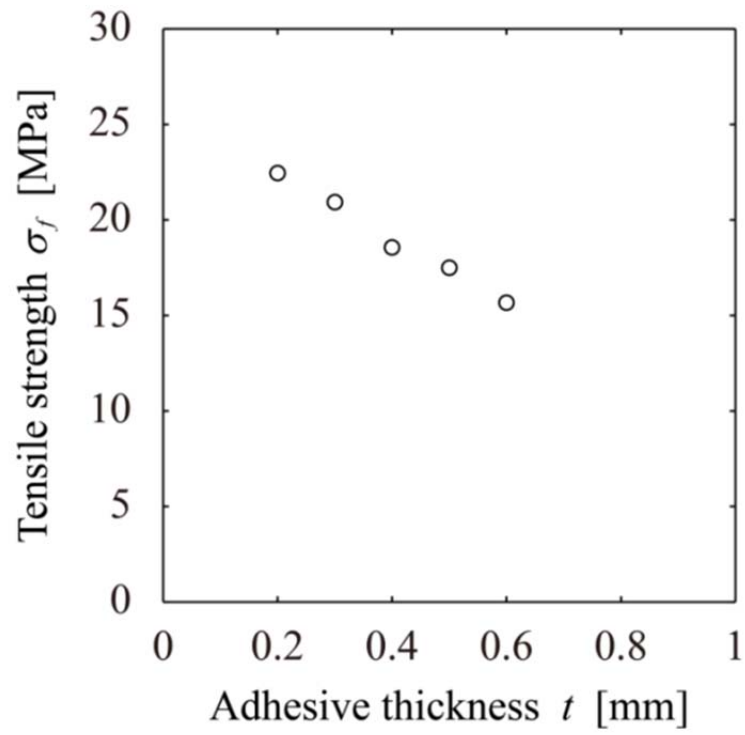


Fig. A2 Relation between the tensile strength σ_f and adhesive thickness t

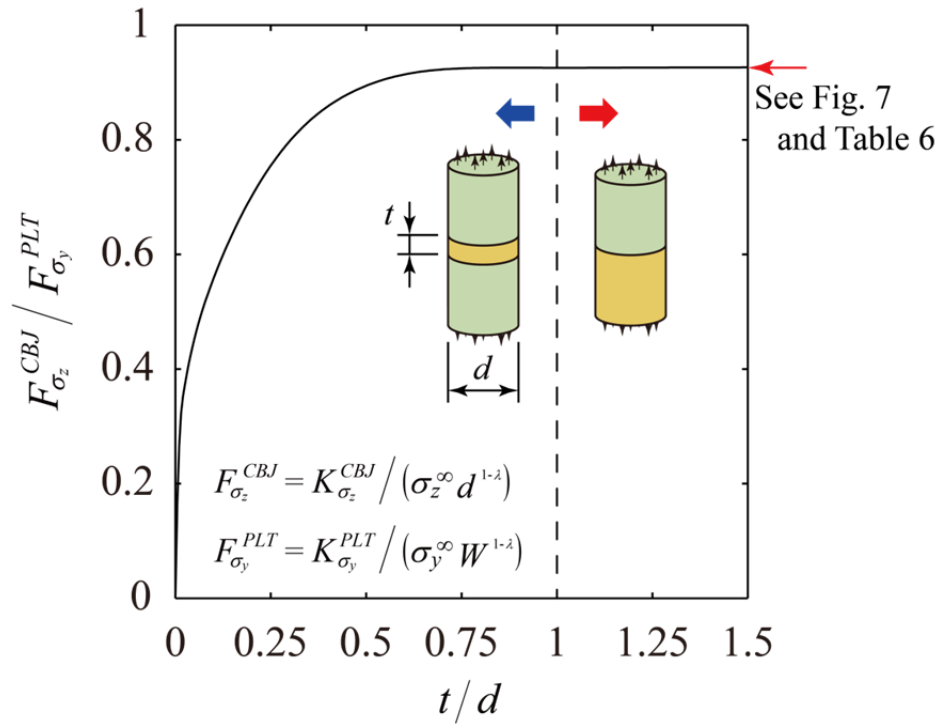


Fig. A3 Dimensionless ISSF for the cylindrical butt joint, $F_{\sigma_z}^{CBJ}$

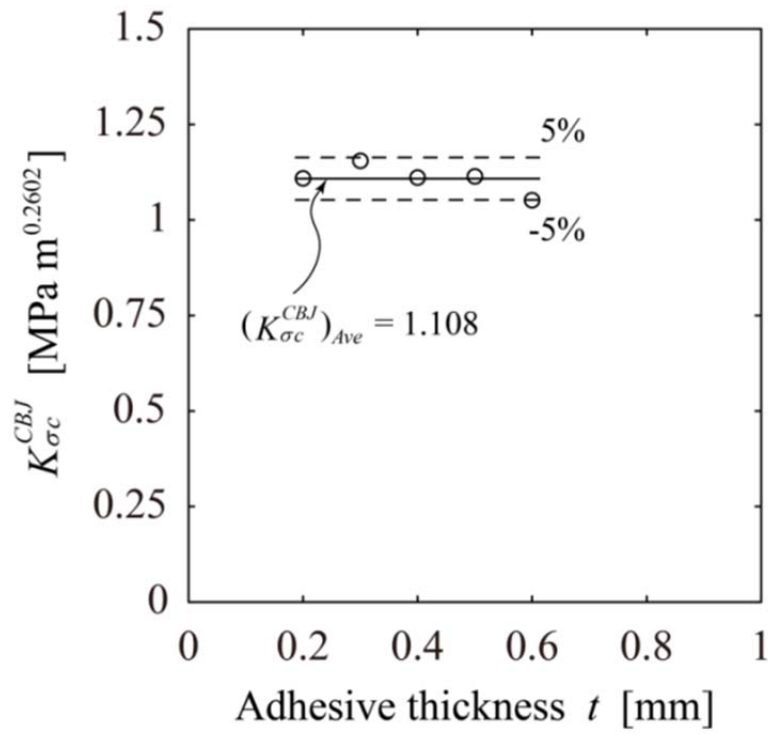


Fig. A4 The critical ISSF, $K_{\sigma_c}^{CBJ}$

Table 1 An example of bad pair $(\alpha, \beta) = (0.8, 0.3)$ satisfying $\alpha(\alpha - 2\beta) > 0$ used to explain the present analysis

Material 1		Material 2		α	β	λ
E_1	ν_1	E_2	ν_2			
1.0	0.2555	0.1138	0.2066	0.8	0.3	0.8655

Table 2 Mesh-dependent FEM stress / strain at the interface end when $(\alpha, \beta) = (0.8, 0.3)$ and $\nu_1 = 0.2555$ in Table 1

(a) Bonded cylinder (Mesh-dependent except for ε_θ)

Stress components (= singular stress + non-singular stress)								
$\frac{e_{\min}}{a}$	$\sigma_{r,0,FEM}^{CYL}$		$\sigma_{z,0,FEM}^{CYL}$		$\sigma_{\theta,0,FEM}^{CYL}$		$\tau_{rz,0,FEM}^{CYL}$	
	Mat. 1	Mat. 2	Mat. 1	Mat. 2	Mat. 1	Mat. 2	Mat. 1	Mat. 2
3^{-9}	-0.6785 (= -0.6785 + 0.0)	0.6515 (= 0.6515 + 0.0)	3.561 (= 3.575 - 0.01344)		0.2803 (= 0.7974 - 0.5171)	0.7653 (= 0.8265 - 0.06124)	0.3210 (= 0.3210 + 0.0)	
3^{-12}	-1.057 (= -1.057 + 0.0)	1.015 (= 1.015 + 0.0)	5.555 (= 5.569 - 0.01344)		0.7251 (= 1.242 - 0.5172)	1.226 (= 1.288 - 0.06124)	0.5000 (= 0.5000 + 0.0)	
Strain components (= singular strain + non-singular strain)								
$\frac{e_{\min}}{a}$	$\varepsilon_{r,0,FEM}^{CYL}$		$\varepsilon_{z,0,FEM}^{CYL}$		$\varepsilon_{\theta,0,FEM}^{CYL}$		$\gamma_{rz,0,FEM}^{CYL}$	
	$\left[\frac{\sigma_{r,0,FEM}^{CYL} - \nu(\sigma_{\theta,0,FEM}^{CYL} + \sigma_{z,0,FEM}^{CYL})}{E} \right]$		$\left[\frac{\sigma_{z,0,FEM}^{CYL} - \nu(\sigma_{r,0,FEM}^{CYL} + \sigma_{\theta,0,FEM}^{CYL})}{E} \right]$		$\left[\frac{\sigma_{\theta,0,FEM}^{CYL} - \nu(\sigma_{z,0,FEM}^{CYL} + \sigma_{r,0,FEM}^{CYL})}{E} \right]$		$\left[\frac{\tau_{rz,0,FEM}^{CYL}}{G} \right]$	
	Mat. 1	Mat. 2	Mat. 1	Mat. 2	Mat. 1	Mat. 2	Mat. 1	Mat. 2
3^{-9}	-1.719 (= -1.854 + 0.1356)		3.888 (= 3.769 + 0.1187)	26.75 (= 26.75 - 0.006950)	-0.5137 (= 0.0 - 0.5137)		0.2105 (= 0.2105 + 0.0)	11.83 (= 11.83 + 0.0)
3^{-12}	-2.753 (= -2.889 + 0.1356)		5.991 (= 5.872 + 0.1187)	41.67 (= 41.67 - 0.006950)	-0.5137 (= 0.0 - 0.5137)		0.3282 (= 0.3282 + 0.0)	18.43 (= 18.43 + 0.0)

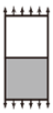


$$\sigma_{z,0,FEM}^{CYL} = \left\{ (\sigma_{z,0,FEM}^{CYL})^1 + (\sigma_{z,0,FEM}^{CYL})^2 \right\} / 2, \quad \tau_{rz,0,FEM}^{CYL} = \left\{ (\tau_{rz,0,FEM}^{CYL})^1 + (\tau_{rz,0,FEM}^{CYL})^2 \right\} / 2 \text{ for continuity of stress}$$

$$\varepsilon_{r,0,FEM}^{CYL} = \left\{ (\varepsilon_{r,0,FEM}^{CYL})^1 + (\varepsilon_{r,0,FEM}^{CYL})^2 \right\} / 2, \quad \varepsilon_{\theta,0,FEM}^{CYL} = \left\{ (\varepsilon_{\theta,0,FEM}^{CYL})^1 + (\varepsilon_{\theta,0,FEM}^{CYL})^2 \right\} / 2 \text{ for continuity of strain}$$

(b) Bonded plate (Mesh-dependent except for ε_z)

Stress components [= singular stress + non-singular stress (=0)]								
$\frac{e_{\min}}{a}$	$\sigma_{x,0,FEM}^{PLT}$		$\sigma_{y,0,FEM}^{PLT}$		$\sigma_{z,0,FEM}^{PLT}$		$\tau_{xy,0,FEM}^{PLT}$	
	Mat. 1	Mat. 2	Mat. 1	Mat. 2	Mat. 1	Mat. 2	Mat. 1	Mat. 2
3^{-9}	-0.6821 (= -0.6821 + 0.0)	0.6549 (= 0.6549 + 0.0)	3.593 (= 3.593 + 0.0)		0.8016 (= 0.8016 + 0.0)	0.8308 (= 0.8308 + 0.0)	0.3226 (= 0.3226 + 0.0)	
3^{-12}	-1.063 (= -1.063 + 0.0)	1.020 (= 1.020 + 0.0)	5.598 (= 5.598 + 0.0)		1.249 (= 1.249 + 0.0)	1.294 (= 1.294 + 0.0)	0.5026 (= 0.5026 + 0.0)	
Strain components (= singular strain + non-singular strain)								
$\frac{e_{\min}}{a}$	$\varepsilon_{x,0,FEM}^{PLT}$		$\varepsilon_{y,0,FEM}^{PLT}$		$\varepsilon_{z,0,FEM}^{PLT}$		$\gamma_{xy,0,FEM}^{PLT}$	
	$\left[\frac{\sigma_{x,0,FEM}^{PLT} - \nu(\sigma_{y,0,FEM}^{PLT} + \sigma_{z,0,FEM}^{PLT})}{E} \right]$		$\left[\frac{\sigma_{y,0,FEM}^{PLT} - \nu(\sigma_{x,0,FEM}^{PLT} + \sigma_{z,0,FEM}^{PLT})}{E} \right]$		$\left[\frac{\sigma_{z,0,FEM}^{PLT} - \nu(\sigma_{x,0,FEM}^{PLT} + \sigma_{y,0,FEM}^{PLT})}{E} \right]$		$\left[\frac{\tau_{xy,0,FEM}^{PLT}}{G} \right]$	
	Mat. 1	Mat. 2	Mat. 1	Mat. 2	Mat. 1	Mat. 2	Mat. 1	Mat. 2
3^{-9}	-1.864 (= -1.864 + 0.0)		3.789 (= 3.789 + 0.0)	4.347 (= 4.347 + 0.0)	0.0 (= 0.0 + 0.0)		0.2118 (= 0.2118 + 0.0)	11.90 (= 11.90 + 0.0)
3^{-12}	-2.904 (= -2.904 + 0.0)		5.903 (= 5.903 + 0.0)	6.772 (= 6.772 + 0.0)	0.0 (= 0.0 + 0.0)		0.3299 (= 0.3299 + 0.0)	18.53 (= 18.53 + 0.0)



$$\sigma_{y,0,FEM}^{PLT} = \left\{ (\sigma_{y,0,FEM}^{PLT})^1 + (\sigma_{y,0,FEM}^{PLT})^2 \right\} / 2, \quad \tau_{xy,0,FEM}^{PLT} = \left\{ (\tau_{xy,0,FEM}^{PLT})^1 + (\tau_{xy,0,FEM}^{PLT})^2 \right\} / 2 \text{ for continuity of stress}$$

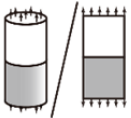
$$\varepsilon_{x,0,FEM}^{PLT} = \left\{ (\varepsilon_{x,0,FEM}^{PLT})^1 + (\varepsilon_{x,0,FEM}^{PLT})^2 \right\} / 2, \quad \varepsilon_{z,0,FEM}^{PLT} = \left\{ (\varepsilon_{z,0,FEM}^{PLT})^1 + (\varepsilon_{z,0,FEM}^{PLT})^2 \right\} / 2 \text{ for continuity of strain}$$

Table 3 Mesh-independent $\varepsilon_{\theta 0, FEM}^{CYL}$ values obtained by $u_{r 0, FEM}^{CYL}$ and $\sigma_{j 0, FEM}^{CYL}$ (=singular strain + non-singular strain) when $(\alpha, \beta) = (0.8, 0.3)$ and $\nu_1 = 0.2555$ in Table 1

$\frac{e_{\min}}{a}$	$\varepsilon_{\theta 0, FEM}^{CYL} \left[= \frac{u_{r, FEM}^{CYL}}{r} \Big _{r=a} \right]$	$\varepsilon_{\theta 0, FEM}^{CYL} \left[= \frac{\sigma_{\theta 0, FEM}^{CYL} - \nu(\sigma_{z 0, FEM}^{CYL} + \sigma_{r 0, FEM}^{CYL})}{E} \right]$
3^{-9}	-0.5137	-0.5137 (= 0.0 - 0.5137)
3^{-12}	-0.5137	-0.5137 (= 0.0 - 0.5137)

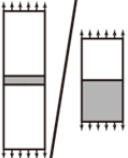
Table 4 FEM stress ratio for the bonded cylinder when $(\alpha, \beta) = (0.8, 0.3)$ and $\nu_1 = 0.2555$ in Table 1 [= (singular stress + non-singular stress) / singular stress] (See Sect. 2.3)

(a) Bonded cylinder / bonded plate (Mesh-independent if non-singular stress is zero)



$\frac{e_{\min}}{a}$	$\frac{\sigma_{r0,FEM}^{CYL}}{\sigma_{x0,FEM}^{PLT}}$		$\frac{\sigma_{z0,FEM}^{CYL}}{\sigma_{y0,FEM}^{PLT}}$		$\frac{\sigma_{\theta 0,FEM}^{CYL}}{\sigma_{z0,FEM}^{PLT}}$		$\frac{\tau_{rz0,FEM}^{CYL}}{\tau_{xy0,FEM}^{PLT}}$	
	Mat. 1	Mat. 2	Mat. 1	Mat. 2	Mat. 1	Mat. 2	Mat. 1	Mat. 2
3^{-9}	0.9948 $\left(= \frac{-0.6785 + 0.0}{-0.6821} \right)$	0.9948 $\left(= \frac{0.6515 + 0.0}{0.6549} \right)$	0.9911 $\left(= \frac{3.575 - 0.01344}{3.593} \right)$		0.3497 $\left(= \frac{0.7974 - 0.5171}{0.8016} \right)$	0.9211 $\left(= \frac{0.8265 - 0.06124}{0.8308} \right)$	0.9948 $\left(= \frac{0.3210 + 0.0}{0.3226} \right)$	
3^{-12}	0.9948 $\left(= \frac{-1.057 + 0.0}{-1.063} \right)$	0.9948 $\left(= \frac{1.015 + 0.0}{1.020} \right)$	0.9924 $\left(= \frac{5.569 - 0.01344}{5.598} \right)$		0.5807 $\left(= \frac{1.242 - 0.5172}{1.249} \right)$	0.9475 $\left(= \frac{1.288 - 0.06124}{1.294} \right)$	0.9948 $\left(= \frac{0.5000 + 0.0}{0.5026} \right)$	

(b) Butt joint / bonded plate (Mesh-independent because non-singular stress is always zero)



$\frac{e_{\min}}{a}$	$\frac{\sigma_{x0,FEM}^{BJ}}{\sigma_{x0,FEM}^{PLT}}$		$\frac{\sigma_{y0,FEM}^{BJ}}{\sigma_{y0,FEM}^{PLT}}$		$\frac{\sigma_{z0,FEM}^{BJ}}{\sigma_{z0,FEM}^{PLT}}$		$\frac{\tau_{xy0,FEM}^{BJ}}{\tau_{xy0,FEM}^{PLT}}$	
	Mat. 1	Mat. 2	Mat. 1	Mat. 2	Mat. 1	Mat. 2	Mat. 1	Mat. 2
3^{-9}	0.6745 $\left(= \frac{-0.4601 + 0.0}{-0.6821} \right)$	0.6745 $\left(= \frac{0.4417 + 0.0}{0.6549} \right)$	0.6746 $\left(= \frac{2.424 + 0.0}{3.593} \right)$		0.6747 $\left(= \frac{0.5408 + 0.0}{0.8016} \right)$	0.6746 $\left(= \frac{0.5604 + 0.0}{0.8308} \right)$	0.6750 $\left(= \frac{0.2178 + 0.0}{0.3226} \right)$	
3^{-12}	0.6746 $\left(= \frac{-0.7168 + 0.0}{-1.063} \right)$	0.6747 $\left(= \frac{0.6883 + 0.0}{1.020} \right)$	0.6747 $\left(= \frac{3.777 + 0.0}{5.598} \right)$		0.6747 $\left(= \frac{0.8425 + 0.0}{1.249} \right)$	0.6747 $\left(= \frac{0.8732 + 0.0}{1.294} \right)$	0.6747 $\left(= \frac{0.3391 + 0.0}{0.5026} \right)$	

(c) FEM stress of butt joint [= singular stress + non-singular stress (= 0)] (Mesh-dependent)



$\frac{e_{\min}}{a}$	$\sigma_{x0,FEM}^{BJ}$		$\sigma_{y0,FEM}^{BJ}$		$\sigma_{z0,FEM}^{BJ}$		$\tau_{xy0,FEM}^{BJ}$	
	Mat. 1	Mat. 2	Mat. 1	Mat. 2	Mat. 1	Mat. 2	Mat. 1	Mat. 2
3^{-9}	-0.4601 $(= -0.4601 + 0.0)$	0.4417 $(= 0.4417 + 0.0)$	2.424 $(= 2.424 + 0.0)$		0.5408 $(= 0.5408 + 0.0)$	0.5604 $(= 0.5604 + 0.0)$	0.2178 $(= 0.2178 + 0.0)$	
3^{-12}	-0.7168 $(= -0.7168 + 0.0)$	0.6883 $(= 0.6883 + 0.0)$	3.777 $(= 3.777 + 0.0)$		0.8425 $(= 0.8425 + 0.0)$	0.8732 $(= 0.8732 + 0.0)$	0.3391 $(= 0.3391 + 0.0)$	

$$\sigma_{y0,FEM}^{BJ} = \left\{ (\sigma_{y0,FEM}^{BJ})^2 + (\sigma_{z0,FEM}^{BJ})^2 \right\} / 2, \quad \tau_{xy0,FEM}^{BJ} = \left\{ (\tau_{xy0,FEM}^{BJ})^2 + (\tau_{xz0,FEM}^{BJ})^2 \right\} / 2 \text{ for continuity of stress}$$

Table 5 FEM stress ratio by excluding non-singular stress (a) as shown in Table 5(c) when $(\alpha, \beta) = (0.8, 0.3)$ and $\nu_1 = 0.2555$ in Table 1

(a) Non-singular FEM stress of the bonded cylinder obtained by using explicit Eqs. (14), (15), (18), (19), (20) (Mesh-independent)

$\frac{e_{\min}}{a}$	$\tilde{\sigma}_{r0,FEM}^{CYL}$		$\tilde{\sigma}_{z0,FEM}^{CYL}$		$\tilde{\sigma}_{\theta0,FEM}^{CYL}$		$\tilde{\tau}_{rz0,FEM}^{CYL}$	
	Mat. 1	Mat. 2	Mat. 1	Mat. 2	Mat. 1	Mat. 2	Mat. 1	Mat. 2
3^{-9}	0.0	0.0	-0.01344		-0.5171	-0.06124	0.0	
3^{-12}	0.0	0.0	-0.01344		-0.5172	-0.06124	0.0	

(b) Singular FEM stress of the bonded cylinder by excluding non-singular stress in Table 5 (a) (Mesh-dependent)

$\frac{e_{\min}}{a}$	$\sigma_{r0,FEM}^{CYL} - \tilde{\sigma}_{r0,FEM}^{CYL}$		$\sigma_{z0,FEM}^{CYL} - \tilde{\sigma}_{z0,FEM}^{CYL}$		$\sigma_{\theta0,FEM}^{CYL} - \tilde{\sigma}_{\theta0,FEM}^{CYL}$		$\tau_{rz0,FEM}^{CYL} - \tilde{\tau}_{rz0,FEM}^{CYL}$	
	Mat. 1	Mat. 2	Mat. 1	Mat. 2	Mat. 1	Mat. 2	Mat. 1	Mat. 2
3^{-9}	-0.6785	0.6515	3.575		0.7974	0.8265	0.3210	
3^{-12}	-1.057	1.015	5.569		1.242	1.288	0.5000	

(c) FEM stress ratio of the bonded cylinder over the bonded plate (Mesh-independent quite differently from Table 4(a) by excluding the non-singular stress in Table 5 (a))

$\frac{e_{\min}}{a}$	$\frac{\sigma_{r0,FEM}^{CYL} - \tilde{\sigma}_{r0,FEM}^{CYL}}{\sigma_{x0,FEM}^{PLT}}$		$\frac{\sigma_{z0,FEM}^{CYL} - \tilde{\sigma}_{z0,FEM}^{CYL}}{\sigma_{y0,FEM}^{PLT}}$		$\frac{\sigma_{\theta0,FEM}^{CYL} - \tilde{\sigma}_{\theta0,FEM}^{CYL}}{\sigma_{z0,FEM}^{PLT}}$		$\frac{\tau_{rz0,FEM}^{CYL} - \tilde{\tau}_{rz0,FEM}^{CYL}}{\tau_{xy0,FEM}^{PLT}}$	
	Mat. 1	Mat. 2	Mat. 1	Mat. 2	Mat. 1	Mat. 2	Mat. 1	Mat. 2
3^{-9}	0.9948	0.9948	0.9948		0.9948	0.9948	0.9948	
3^{-12}	0.9948	0.9948	0.9948		0.9948	0.9948	0.9948	

(d) Dimensionless ISSFs in Eq. (21) and Eq. (22) obtained from the unique ratio in Table 5 (c)

Mat.	Bonded cylinder				Bonded plate			
	$F_{\sigma_r}^{CYL}$	$F_{\sigma_z}^{CYL}$	$F_{\sigma_\theta}^{CYL}$	$F_{\tau_{rz}}^{CYL}$	$F_{\sigma_x}^{PLT}$	$F_{\sigma_y}^{PLT}$	$F_{\sigma_z}^{PLT}$	$F_{\tau_{xy}}^{PLT}$
1	-0.269	0.633	0.0929	0.0958	-0.270	0.636	0.0934	0.0963
2	0.111		0.154		0.111		0.154	

(e) Mesh-independent FEM stress ratio also independent of distance R in Fig. 2 and Fig. 3

$\frac{R}{e_{\min}}$	$\sigma_{z,FEM}^{CYL}$	$\sigma_{y,FEM}^{PLT}$	$\frac{\sigma_{z,FEM}^{CYL} - \tilde{\sigma}_{z0,FEM}^{CYL}}{\sigma_{y,FEM}^{PLT}}$
0	5.555	5.598	0.9948
1	4.064	4.099	0.9948
2	3.754	3.787	0.9948
3	3.571	3.603	0.9948
4	3.449	3.481	0.9948
5	3.356	3.387	0.9948

$$\tilde{\sigma}_{z0,FEM}^{CYL} = -0.01344$$

Table 6 Maximum and minimum values of $K_{\sigma_z}^{CYL} / K_{\sigma_y}^{PLT}$

		β							
		-0.2	-0.1	0	0.1	0.2	0.3	0.4	0.45
α	0.1	0.789	0.855	0.996					
		0.781	0.835	0.896					
	0.2	0.775	0.861	0.986					
			0.825	0.885					
	0.3		0.856	0.972	1.234				
			0.814	0.870	0.944				
	0.4		0.845	0.955	1.084				
			0.808	0.854	0.916				
	0.5		0.827	0.937	1.022	1.346			
			0.804	0.843	0.895	0.962			
0.6		0.802	0.918	0.981	1.121				
			0.837	0.880	0.936				
0.7			0.899	0.948	1.032	1.321			
			0.833	0.870	0.918	0.976			
0.8			0.879	0.919	0.977	1.089			
			0.832	0.865	0.906	0.957			
0.9			0.859	0.892	0.935	0.996	1.146		
			0.834	0.863	0.899	0.944	0.992		
1			0.839	0.866	0.898	0.937	0.981	0.995	

Upper: maximum value, lower: minimum value

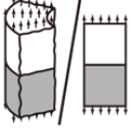
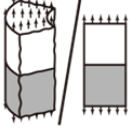
Table 7 Maximum and minimum values of $\sigma_{z0,FEM}^{CYL} / \sigma_{y0,FEM}^{PLT}$

		β							
		-0.2	-0.1	0	0.1	0.2	0.3	0.4	0.45
α	0.0	0.987 0.948	0.997 0.981	1.000	0.997 0.981	0.978 0.948			
	0.1	0.903 0.878	0.956 0.936	0.996 0.989	1.032 1.000	1.065 1.022			
	0.2	0.844	0.920 0.896	0.986 0.955	1.052 1.000	1.145 1.060	1.246		
	0.3		0.889 0.850	0.972 0.914	1.050 0.984	1.184 1.036	1.444 1.358		
	0.4		0.863 0.826	0.955 0.880	1.031 0.948	1.172 1.000	1.525 1.343		
	0.5		0.838 0.812	0.937 0.857	1.000 0.914	1.127 0.983	1.447 1.134		
	0.6		0.808	0.918 0.843	0.975 0.890	1.071 0.951	1.299 1.000	3.117	
	0.7			0.899 0.835	0.946 0.875	1.020 0.925	1.165 0.986	1.862 1.564	
	0.8			0.879 0.833	0.919 0.866	0.974 0.909	1.066 0.962	1.327 1.000	2.276
	0.9			0.859 0.834	0.892 0.864	0.934 0.900	0.993 0.945	1.098 0.994	1.237 1.000
	1			0.839	0.866	0.898	0.937	0.981	0.995

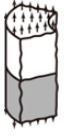
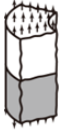
Upper: maximum value, lower: minimum value

Table 8 FEM stress ratio for the bonded pipe when $(\alpha, \beta) = (0.8, 0.3)$ and $\nu_1 = 0.2555$ in Table 1
 [= (singular stress + non-singular stress) / singular stress]

(a) Bonded pipe / bonded plate (Mesh-independent if non-singular stress is zero)

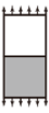
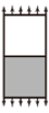
	$\frac{e_{\min}}{W/2}$	$\sigma_{r0,FEM}^{PIP} / \sigma_{x0,FEM}^{PLT}$		$\sigma_{z0,FEM}^{PIP} / \sigma_{y0,FEM}^{PLT}$		$\sigma_{\theta 0,FEM}^{PIP} / \sigma_{z0,FEM}^{PLT}$		$\tau_{rz0,FEM}^{PIP} / \tau_{xy0,FEM}^{PLT}$	
		Mat. 1	Mat. 2	Mat. 1	Mat. 2	Mat. 1	Mat. 2	Mat. 1	Mat. 2
	2^{-13}	1.021 $(= \frac{-0.7412+0.0}{-0.7261})$	1.021 $(= \frac{0.4562+0.0}{0.4469})$	1.014 $(= \frac{3.031-0.0193}{2.970})$		-0.1284 $(= \frac{0.6598-0.7428}{0.6465})$	0.8847 $(= \frac{0.6600-0.0880}{0.6465})$	1.021 $(= \frac{0.2008+0.0}{0.1967})$	
	2^{-17}	1.020 $(= \frac{-1.076+0.0}{-1.054})$	1.020 $(= \frac{0.6622+0.0}{0.6490})$	1.016 $(= \frac{4.400-0.0193}{4.312})$		0.2291 $(= \frac{0.9578-0.7427}{0.9387})$	0.9268 $(= \frac{0.9579-0.0879}{0.9388})$	1.020 $(= \frac{0.2913+0.0}{0.2855})$	

(b) FEM stress of bonded pipe (Mesh-dependent) [= singular stress + non-singular stress]

	$\frac{e_{\min}}{W/2}$	$\sigma_{r0,FEM}^{PIP}$		$\sigma_{z0,FEM}^{PIP}$		$\sigma_{\theta 0,FEM}^{PIP}$		$\tau_{rz0,FEM}^{PIP}$	
		Mat. 1	Mat. 2	Mat. 1	Mat. 2	Mat. 1	Mat. 2	Mat. 1	Mat. 2
	2^{-13}	-0.7412 $(= -0.7412 + 0.0)$	0.4562 $(= 0.4562 + 0.0)$	3.012 $(= 3.031 - 0.0193)$		-0.0830 $(= 0.6598 - 0.7428)$	0.5720 $(= 0.6600 - 0.0880)$	0.2008 $(= 0.2008 + 0.0)$	
	2^{-17}	-1.076 $(= -1.076 + 0.0)$	0.6622 $(= 0.6622 + 0.0)$	4.381 $(= 4.400 - 0.0193)$		0.2151 $(= 0.9578 - 0.7427)$	0.8700 $(= 0.9579 - 0.0879)$	0.2913 $(= 0.2913 + 0.0)$	

$$\sigma_{z0,FEM}^{PIP} = \left\{ (\sigma_{z0,FEM}^{PIP})^2 + (\sigma_{z0,FEM}^{PIP})^2 \right\} / 2, \quad \tau_{rz0,FEM}^{PIP} = \left\{ (\tau_{rz0,FEM}^{PIP})^2 + (\tau_{rz0,FEM}^{PIP})^2 \right\} / 2 \text{ for continuity of stress}$$

(c) FEM stress of bonded plate (Mesh-dependent) [= singular stress + non-singular stress (= 0)]

	$\frac{e_{\min}}{W/2}$	$\sigma_{x0,FEM}^{PLT}$		$\sigma_{y0,FEM}^{PLT}$		$\sigma_{z0,FEM}^{PLT}$		$\tau_{xy0,FEM}^{PLT}$	
		Mat. 1	Mat. 2	Mat. 1	Mat. 2	Mat. 1	Mat. 2	Mat. 1	Mat. 2
	2^{-13}	-0.7261 $(= -0.7261 + 0.0)$	0.4469 $(= 0.4469 + 0.0)$	2.970 $(= 2.970 + 0.0)$		0.6465 $(= 0.6465 + 0.0)$	0.6465 $(= 0.6465 + 0.0)$	0.1967 $(= 0.1967 + 0.0)$	
	2^{-17}	-1.054 $(= -1.054 + 0.0)$	0.6490 $(= 0.6490 + 0.0)$	4.312 $(= 4.312 + 0.0)$		0.9387 $(= 0.9387 + 0.0)$	0.9388 $(= 0.9388 + 0.0)$	0.2855 $(= 0.2855 + 0.0)$	

$$\sigma_{y0,FEM}^{PLT} = \left\{ (\sigma_{y0,FEM}^{PLT})^2 + (\sigma_{y0,FEM}^{PLT})^2 \right\} / 2, \quad \tau_{xy0,FEM}^{PLT} = \left\{ (\tau_{xy0,FEM}^{PLT})^2 + (\tau_{xy0,FEM}^{PLT})^2 \right\} / 2 \text{ for continuity of stress}$$

Table 9 FEM stress ratio of the bonded cylinder over the bonded plate (Mesh-independent differently from Table 8(a) by excluding the non-singular stress)

$\frac{e_{\min}}{W/2}$	$\frac{\sigma_{r0,FEM}^{PIP} - \tilde{\sigma}_{r0,FEM}^{PIP}}{\sigma_{x0,FEM}^{PLT}}$		$\frac{\sigma_{z0,FEM}^{PIP} - \tilde{\sigma}_{z0,FEM}^{PIP}}{\sigma_{y0,FEM}^{PLT}}$		$\frac{\sigma_{\theta0,FEM}^{PIP} - \tilde{\sigma}_{\theta0,FEM}^{PIP}}{\sigma_{z0,FEM}^{PLT}}$		$\frac{\tau_{rz0,FEM}^{PIP} - \tilde{\tau}_{rz0,FEM}^{PIP}}{\tau_{xy0,FEM}^{PLT}}$	
	Mat. 1	Mat. 2	Mat. 1	Mat. 2	Mat. 1	Mat. 2	Mat. 1	Mat. 2
2^{-13}	1.021	1.021	1.021		1.021	1.021	1.021	
2^{-17}	1.020	1.020	1.020		1.020	1.020	1.020	

Table 10 Maximum and minimum values of $K_{\sigma_z}^{PIP} / K_{\sigma_y}^{PLT}$

		β							
		-0.2	-0.1	0	0.1	0.2	0.3	0.4	0.45
α	0.1	0.808	0.923	0.999					
		0.807	0.845	0.896					
	0.2	0.794	0.879	0.999					
			0.840	0.888					
	0.3		0.882	1.000	1.249				
			0.832	0.874	0.939				
	0.4		0.879	1.000	1.114				
			0.829	0.862	0.911				
	0.5		0.870	0.999	1.069	1.382			
			0.830	0.856	0.893	0.953			
0.6		0.842	1.002	1.047	1.172				
			0.859	0.884	0.927				
0.7			1.000	1.034	1.101	1.383			
			0.865	0.885	0.915	0.963			
0.8			0.998	1.023	1.064	1.160			
			0.885	0.897	0.916	0.947			
0.9			0.998	1.014	1.035	1.075	1.210		
			0.920	0.927	0.937	0.953	0.980		
1			1.000	1.000	1.000	1.000	1.000	1.000	

Upper: maximum value, lower: minimum value

Table 11 Maximum and minimum values of $\sigma_{z0,FEM}^{PIP} / \sigma_{y0,FEM}^{PLT}$

		β							
		-0.2	-0.1	0	0.1	0.2	0.3	0.4	0.45
α	0.0	0.986 0.975	0.998 0.990	1.000	0.998 0.990	0.986 0.975			
	0.1	0.947 0.931	0.981 0.936	1.000 0.992	1.020 1.002	1.036 1.013			
	0.2	0.904	0.953 0.929	1.000 0.971	1.036 1.000	1.082 1.030	1.098		
	0.3		0.932 0.898	1.000 0.941	1.044 0.988	1.111 1.019	1.191 1.152		
	0.4		0.921 0.875	1.000 0.913	1.045 0.961	1.119 1.000	1.252 1.132		
	0.5		0.898 0.861	1.000 0.892	1.041 0.933	1.111 0.985	1.259 1.059		
	0.6		0.862	1.001 0.880	1.035 0.912	1.093 0.958	1.234 1.000	1.405	
	0.7			1.000 0.878	1.028 0.902	1.073 0.937	1.158 0.976	1.377 1.186	
	0.8			1.000 0.891	1.021 0.906	1.054 0.929	1.109 0.963	1.228 1.000	1.395
	0.9			1.000 0.924	1.013 0.931	1.032 0.942	1.063 0.960	1.116 0.989	1.162 1.000
	1			1.000	1.000	1.000	1.000	1.000	1.000

Upper: maximum value, lower: minimum value

Table A1 Dundurs' parameters (α, β) and singular index λ

Adherend (Al alloy)		Adhesive (Polyimide)		Dundurs' parameter		Singular index
E_1 [GPa]	ν_1	E_2 [GPa]	ν_2	α	β	λ
69.9	0.33	3.77	0.342	0.8963	0.2145	0.7398